Study and design of a novel leaky-wave antenna based on the Substrate Integrated Non-Radiative Dielectric (SINRD) technology

Author: Pedro Fidel Espín López
pedrofi.espin@gmail.com

Director: Alejandro Álvarez Melcón

April 20, 2015

Author	Pedro Fidel Espín López
Author's email	pedrofi.espin@gmail.com
Director	Alejandro Álvarez Melcón
Director's email	alejandro.alvarez@upct.es
Co-director	Fernando D. Quesada Pereira and Maurizio Bozzi
Title	Study and design of a novel leaky-wave antenna based on the Substrate Integrated Non-Radiative Dielectric (SINRD) technology
Summary	This work deals with the design of a planar leaky-wave antenna based on the Substrated Integrated Non-Radiative Dielectric(SINRD) technology. This technology is used in the design of circuits and components at high frequencies. Starting from a known leaky-wave antenna based on non-planar technology, this work develops the study and design of the planar version based on SINRD technology. In addition, as result of these studies, a novel waveguide called aSINRD has been proposed, designed and built. This waveguide presents several improvements and could be a good starting point for future studies based on integrated NRD technologies.
Degree	Ingenierio de Telecomunicación
Department	Tecnologías de la información y la comunicación
Submission Date	April 2015

Abstract

This work deals with the design of a planar leaky-wave antenna based on the Substrated Integrated Non-Radiative Dielectric(SINRD) technology. This technology is used in the design of circuits and components at high frequencies. Starting from a known leaky-wave antenna based on non-planar technology, this work develops the study and design of the planar version based on SINRD technology.

In addition, as result of these studies, a novel waveguide called aSINRD has been proposed, designed and built. This waveguide presents several improvements and could be a good starting point for future studies based on integrated NRD technologies.

Acknowledgements

I want to thank to all my relatives, laboratory colleagues and closest friends for the support they have given to me. Specially to the director of this work, Alejandro Álvarez Melcón for being a good thesis director, which is not easy to find. To my thesis director in Pavia, Maurizio Bozzi, for its hospitable reception in the laboratory. And to Katya Longo for its unconditional support during the development of this work.

Contents

List of Figures

Introduction

A leaky-wave antenna is basically a waveguiding structure which has been physically modified in order to leak power all along its structure [1]. Due to its high directivity and gain, these antennas have been the subject of extensive research since its introduction in 1940 by W. W. Hansen. This early structure consisted of a rectangular waveguide with a continuous slit cut along its side [5], as shown in Figure 1. The topic of leaky-wave antennas did not see a huge growing until the 1950s. From that decade, different types of leaky-wave antennas were introduced, most of them based on closed waveguides structures where the leakage was achieved by introducing long uniform slits.

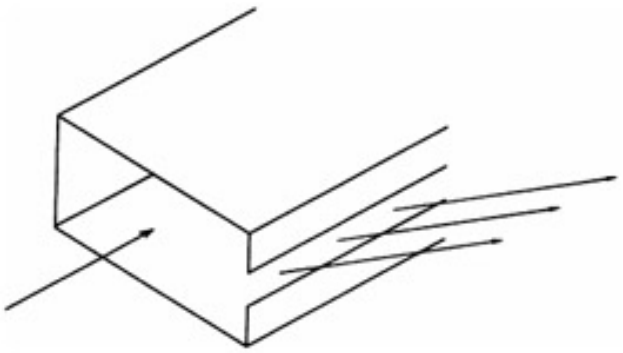

Figure 1: Representation of the first leaky-wave antenna proposed by W. W. Hansen. Reproduced from [1].

Three principal categories had been known in electrical circuitry until the arising of the planar circuits. They were the lumped constant (O-dimensional) circuit, distributed-constant (l-dimensional) circuit, and waveguide (3-dimensional) circuit. Once the planar circuits were introduced, they have been used in a lot of different applications due to its high performance and capability of integrity. A planar circuit can be defined as an electrical

circuit having dimensions comparable to the wavelength in two directions, but with much smaller thickness in one direction"[6].

Combining these two technologies it have been possible to introduce a variety of planar leaky-waves antennas, using for instance the Microstrip technology [7] or the Substrate Integrated Waveguide technology [8]. These antennas present a high directivity and gain due to its leakage nature as well as its capability of integration and reduced dimensions due to its planar structure.

The main goal of this work is to combine these two technologies by designing a planar leaky-wave antenna based on a Substrate Integrate Non-Radiative Dielectric (SINRD) waveguide. The SINRD technology is the planar version of the Non Radiative Dielectric technology (see Fig.2), which was introduced by Yoneyama and Nishida in 1981 [9]. A few years after, a leaky-wave antenna based on this technology was introduced by Oliner and Sanchez [2]. It is the aim of this work to extend the work developed by Oliner and Sanchez into the SINRD planar technology, giving to the antenna the inherent advantages of planar structures.

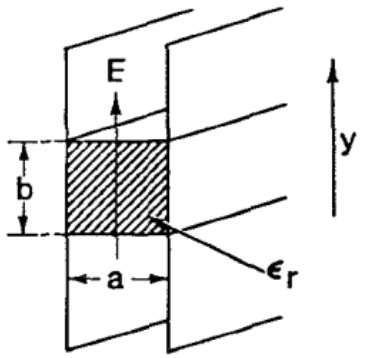

Figure 2: Structure of the Non Radiative Dielectric Waveguide proposed by Yoneyama and Nishida. Reproduced from [2].

In order to achieve this goal, the present work has been divided in several chapters.

Chapter one will present the theoretical basis of the NRD waveguide and it will discuss its application as a leaky-wave antenna. The structure presented by Oliner and Sanchez [2] will be analysed and discussed. Furthermore, the theoretical equations introduced by them will be studied and

a simulator of the structure will be developed. This simulator will help to a better understanding of the structure and it will be, at the same time, a fundamental tool for the final design of a leaky-wave antenna.

In Chapter two the SINRD structure is introduced. The physical layout of the SINRD will be deeply studied and its different ways of designing the structure will be presented. The problems introduced by this structure will be discussed and the different design parameters analysed. To conclude, the simulator implemented in Chapter one will be modified to be able to design a SINRD structure. This simulator will be used to show how the design parameters affect the behaviour of to the final structure.

In Chapter three a leaky-wave antenna based on SINRD technology will be designed at 20 GHz. The whole design process will be explained and the results obtained during the different stages will be shown.

Chapter four is dedicated to the development of a novel SINRD-based waveguide called asymmetric SINRD. This waveguide consist of a physical modification of the SINRD waveguide which adds different advantages such as lower dimensions as compared to the original one. Due to its open nature, the possibility of creating a leaky-wave antenna from this aSINRD by its open face will be presented.

Chapter five, the last one, describes the construction process of a prototype aSINRD waveguide in order to prove its performance. Also the resources of the laboratory where the prototype has been built are described.

Chapter 1

A deep study into the NRD waveguide and its application as a leaky-wave antenna

This chapter is aimed to explain the theory behind the Non Radiative Dielectric (NRD) waveguide structure, how this waveguide can be modified to work as a leaky-wave antenna and finally how a simulator was developed in order to facilitate the design process.

Many sources have been consulted to make this possible, however the most important one was "A New Leaky Waveguide for Millimeter Waves Using Nonradiative Dielectric(NRD) Waveguide- Part I: Accurate Theory" by Alberto Sanchez and Arthur A. Oliner[2] and the references to it will be continuous.

1.1 Accurate theory behind the NRD waveguide

The Nonradiative Dielectric technology was created as a new type of waveguide for millimeter waves with the low losses as its main advantage. The simple but basic modification introduced by Yoneyama and Nishida[9],[11], transformed the old, well-known H guide into a potentially practical waveg-

uide with attractive features. Yoneyama and Nishida observed simply that when the spacing (value of a, see Fig 1.1) is reduced to less than half a wavelength, all the bends and discontinuities become purely reactive and the structure becomes more compact.

These papers [9],[11] treat only reactive circuit components, but no mention is made of how this type of waveguide can be used in conjunction with antennas. This is the purpose of the Sanchez and Oliner paper[2], which will be used as the starting point of this work.

A leaky-wave antenna fabricated with a NRD waveguide

The antenna proposed by Sanchez and Oliner is simple to fabricate since it is composed of a single continuous open slit, and it is fed by a relatively low-loss waveguide so that the leakage constant of the antenna dominates over the attenuation constant of the waveguide due to material losses. The antenna is also simple to design because it is possible to vary the leakage constant without measurably affecting the phase constant[2],[12].

The new waveguide looks like the earlier H guide[13] except that the spacing between the plates is less than half a wavelength to ensure the non-radiative feature. In the vertical (y) direction (see Fig. 1.1), the field is of the standing wave form in the dielectric region and is exponentially decaying in the air regions above and below because of the proximity of the plates. The guided wave propagates in the axial (z) direction(see Fig. 1.1). The antenna is created simply by decreasing the distance d between the dielectric strip and the top of the metal plates. When the distance d is small, the fields have not decayed to negligible values at the upper open end, and, therefore, some power leaks away.

The antenna is analysed as a leaky waveguide that possesses a complex propagation constant $\beta - j\alpha$, where β is the phase constant and α is the attenuation constant or leakage constant. It can be shown that the knowledge of β and α as a function of the geometric parameters is sufficient to permit the complete design of the leaky-wave antenna in accordance with the prescribed radiation requirements. In [2] it is established a transverse equivalent network for the cross section of the antenna, and from the resonant condition of this network we obtain the dispersion relation for the β and α parameters. This transverse equivalent network is shown in Fig.1.2. The reason for the two

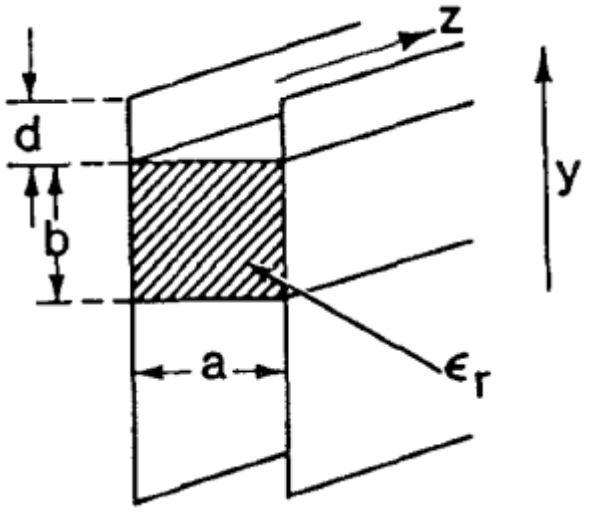

Figure 1.1: Cross section view of the leaky-wave structure where leakage is controlled by the distance *d*. Reproduced from [2].

transmission line sets is that the waveguide modes are hybrid and possess all six field components in the presence of the radiating open end. This is because two sets of modes are coupled at the air dielectric interfaces.

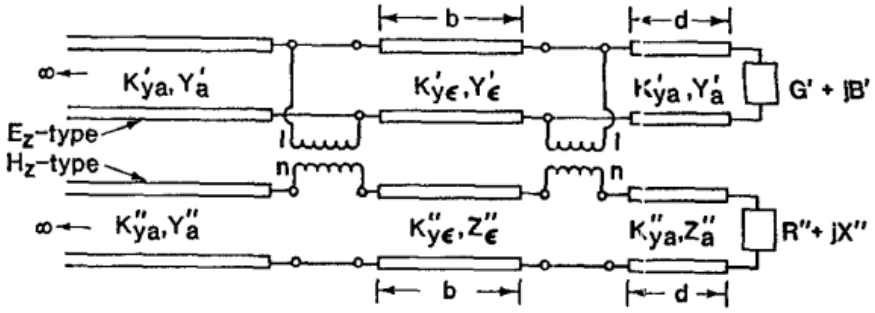

Figure 1.2: Rigorous transverse equivalent network for the structure. Reproduced from [2].

The use of transverse modes

If we employ the usual TE and TM modes in these transmission lines, these will remain uncoupled at the air-dielectric interface but will be coupled together at the radiating open end. On the other hand, the open end is uniform in the longitudinal direction (z-axis, see Fig 1.1), and this geometrical arrangement suggests the use of $E^{(z)} - type$ and $H^{(z)} - type$ (alternative called LSM and LSE modes, respectively, with respect to the xy plane). Transmission lines representing such modes will not couple at the radiating open end, but do become coupled at the air-dielectric interface. The second of these representation is chosen in [2] and it will also be used in this work.

In summary, the final leaky wave propagates in the axial (z) direction (see Fig. 1.1), and the transverse transmission line direction is the vertical (y) direction (see Fig. 1.1). Therefore, the propagation direction of the modes in the transverse equivalent network is thus the y direction. However, the structure is uniform with respect to the z direction. The $E - type$ and $H - type$ modes to be employed in the transverse representation are, therefore, transverse with respect to z, but propagating in y. It is accurate therefore, to designate them as $E^{(z)} - type$ and $H^{(z)} - type$ modes (or alternatively, as LSM and LSE modes with respect to the xy plane).

In [2] they choose the $E - type$ and $H - type$ notation, however in this work it will be retained the notation LSM and LSE as well.

The air-dielectric interface

As it has been explained in the previous section, if the ordinary TE and TM modes were employed in the y direction, the air-dielectric interface would represent a simple junction between transmission lines, and the TE and TM modes would not be coupled together at the interface. For the LSM and LSE modes we employ, however, these modes do couple at the interface, and this coupling has to be studied to complete the analysis. Sanchez and Oliner developed this study in [2]. In summary, the boundary conditions that must be satisfied at the air-dielectric interface (see Fig. 1.3) are

$$E_{t\epsilon} = E_t$$

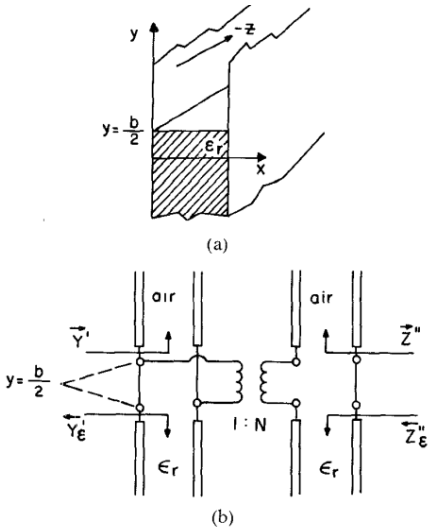

Figure 1.3: (a) Infinite parallel-plate waveguide showing one air-dielectric interface. (b) Transverse equivalent network for the air-dielectric interface in the waveguide shown in (a). Reproduced from [2]

$$H_{t\epsilon} = H_t \tag{1.1}$$

that is, the tangential electric and magnetic fields must be continuous across the interface. Following the development made by Sanchez and Oliner in [2], equation (1.1) becomes

$$(\overleftarrow{Z''_\epsilon} + \overrightarrow{Z''})(\overleftarrow{Y'_\epsilon} + \overrightarrow{Y'}) = N^2 \tag{1.2}$$

where $\overleftarrow{Z''_\epsilon}$ and $\overleftarrow{Y'_\epsilon}$ are the impedance of the LSE mode and the admittance of the LSM mode at the air-dielectric interface looking into the dielectric region, and $\overrightarrow{Z''}$ and $\overrightarrow{Y'}$ are the corresponding quantities looking into the air region. A change in sign results when an impedance or admittance is taken looking in the opposite direction.

A simple network form, shown in Fig. 1.3(b), can be drawn based on (1.2) which is representative of the coupling between the hybrid modes at the air-dielectric interface. The turns ratio N of the transformer is then given by

$$N^2 = \frac{h''_x - h''_{x\epsilon}}{h'_x} \frac{e'_x - e'_{x\epsilon}}{e''_x} \tag{1.3}$$

When the field expressions for the LSE and LSM modes detailed in the Appendix of [2] are used for the modal functions in (1.3) the turns ratio N is obtained as

$$N = \frac{k_0^2(\epsilon_r - 1)\beta(\pi/a)}{(k_0^2 - \beta^2)(\epsilon_r k_0^2 - \beta^2)} \tag{1.4}$$

and the network in Fig. 1.3(b) can be used as a constituent component in a transverse equivalent network that is representative of the NRD guide structure (notice that the leakage phenomenon is not introduced yet).

The radiating open end

Following with the analysis of the structure, if ordinary TE and TM modes with axial (z) variation are incident on the open end of the parallel-plate guide, they become coupled by the discontinuity. The modes remain uncoupled, though, when LSE and LSM modes are employed instead. In obtaining the terminal complex immittances for these modes, which are needed in the transverse equivalent network, Sanchez and Oliner make use of the expressions for reflection coefficients derived by Weinstein [14] for a simpler situation.

His results apply to propagating TM_1 and TE_1 modes in parallel-plate guide normally incident on the radiating open end. The NRD involves modes with longitudinal variation along z which are below cutoff, so that it was necessary to analytically continue Weinstein's results in an appropriate manner.

The analytical continuation made by Sanchez and Oliner required two steps. First, for the NRD guide it is necessary to maintain plate spacing of less than half a wavelength so that the incident modes will be below cutoff in the absence of axial variation. This circumstance calls for an analytic continuation of Weinstein's reflection coefficients to modes below cutoff.

The next step accounts for the longitudinal variation of the incident hy-

brid modes. These modes become the normally incident TE_1 and TM_1 modes when $\beta = 0$. The paper by Altschuler and Goldstone[15] has indicated how reflection coefficients must be modified when a longitudinal variation is introduced into the LSE and LSM modes, provided that these modes remain uncoupled by the discontinuity in question, as is the case of this analysis. The modification is simply to replace k_0 wherever it appears by $(k_0^2 - \beta^2)^{1/2}$.

In Weinstein's notation, the reflection coefficients (referenced to the $\vec{Y}_a'$ and $\vec{Z}_a'$ impedances shown in Fig. 1.5) are written as:

$$R_{1,1} = -|R_{1,1}|e^{-j\theta} \tag{1.5}$$

where

$$|R_{1,1}|_{H1} = \sqrt{(q-\gamma)/(q+\gamma)}e^{-\pi\gamma} = |R''_{1,1}| \tag{1.6}$$

$$|R_{1,1}|_{E1} = \sqrt{(q+\gamma)/(q-\gamma)}e^{-\pi\gamma} = |R'_{1,1}| \tag{1.7}$$

and

$$q = a/\lambda \qquad \gamma = k_y(a/2\pi) = \sqrt{q^2 - 1/4} \tag{1.8}$$

The phase of the reflection coefficient θ is given for both mode types by the next complex equation, also showed in [2],

$$\begin{aligned} \theta &= 2[2 - C + \ln(2/q) - (1/2\gamma)sin^{-1}(\gamma/q) \\ &- (1/\gamma)sin^{-1}(\gamma/\sqrt{2}) + \sigma - \sum_{m=1}^{m=\infty} A_{2m+1}S_m\gamma^{2m}] \end{aligned} \tag{1.9}$$

where

$$\begin{aligned} C &= 0.577... = \lim_{N\to\infty}(\sum_{m=1}^{m=N} 1/n - \ln N) \\ \sigma &= 0.265... = \sum_{n=3}^{n=\infty}[1/(n-1) - 1/\sqrt{n(n-1)}] \end{aligned} \tag{1.10}$$

and A_{2m+1} are the coefficients of the series

$$sin^{-1}x = \sum_{m=0}^{m=\infty} A_{2m+1}x^{2m+1} \tag{1.11}$$

where $A_1 = 1$, $A_3 = 1/6$, $A_5 = 3/40$... and S_m is given by

$$S_m = \sum_{n=3}^{n=\infty} 1/[n(n-1)]^{m+1/2} \tag{1.12}$$

with $S_1 = 0.123$, $S_2 = 0.014$,...

The next step is to relate these reflection coefficients for the wall current densities to the modal voltage and current reflection coefficients corresponding to our transmission line formulation. For the TE_1 (or H_1) mode

$$j_z = H_y|_{wall} = (1/j\omega\mu)\nabla_t \cdot (y_0 \times E_t) \tag{1.13}$$

where the time dependence is $\exp(j\omega\mu)$. Since

$$E_t = V(y)e_t(x) \tag{1.14}$$

we see that the reflection coefficient for the current density j_z is also the voltage reflection coefficient. Consequently,

$$R''_V = -|R''_{1,1}|e^{-j\theta} \tag{1.15}$$

in the same way, for the TM_1 mode,

$$R'_I = -|R'_{1,1}|e^{-j\theta} \tag{1.16}$$

where the modules and phases are still given by (1.6),(1.7) and (1.9).

As it has been said, the work carried out by Sanchez and Oliner[2] is to analytically continue the expression for the reflection coefficients so that they

apply to *modes below cutoff*, taking now the term γ as an imaginary number. The mapping of the terms is shown in Fig. 1.4, where

$$\sqrt{(q \mp \gamma)/(q \pm \gamma)} = \sqrt{(k_0 \mp k_y)/(k_0 \pm k_y)} \equiv \frac{r''_{1,1}}{r'_{1,1}} \tag{1.17}$$

being $r''_{1,1}$ and $r'_{1,1}$ complex numbers.

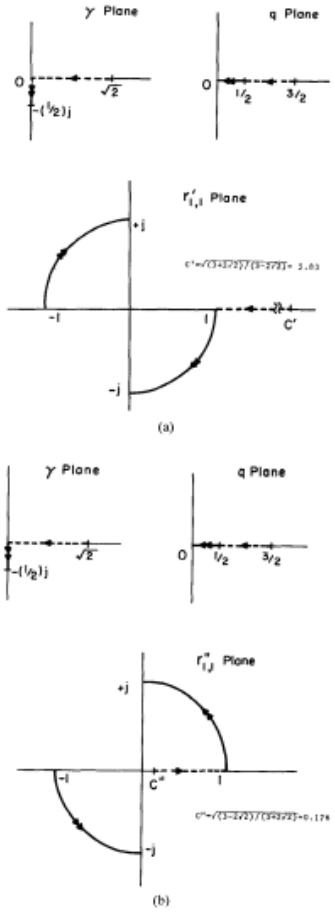

Figure 1.4: (*a*) The q to γ and q to $r'_{1,1}$ mappings. (*b*) The q to γ and q to $r''_{1,1}$ mappings.

Because of this complex nature, at the time of developing the equations, it has to be assured that the values for the terms $r'_{1,1}$ and $r''_{1,1}$ are hold in the same complex quadrant of the theoretical development (see Fig. 1.4). In order to carry out this work, the term γ is bounded to be negative complex, the term $r'_{1,1}$ is bounded to move in the second and fourth quadrant and the term $r''_{1,1}$ in the first and third quadrant as shown in Fig. 1.4.

Once it has been taken into account this, the equations can be adapted to work with the modes LSE and LSM of the NRD waveguide. In order to achieve this the q factor is changed to q', where

$$q = k_0(a/2\pi) \quad q' = (k_0^2 - \beta^2)^{1/2}(a/2\pi) \tag{1.18}$$

When this transformation has been made, the implementation of the radiating open end can follow as Sanchez and Oliner[2] paper details with a correction. Because of the complex nature of the values $r'_{1,1}$ and $r''_{1,1}$, the phase of these factors has to be added to the initial phase detailed in (1.9). This correction is not included in the study of the Oliner and Sanchez paper and the author of this work thinks that it is crucial for the development of the equations. The transformation is as follows:

$$R_{1,1}\Big|_{q'} = -|R_{1,1}|e^{-j\theta}\Big|_{q'} = -|r_{1,1}|e^{-j(\theta+\pi\gamma+\angle r_{1,1})} \tag{1.19}$$

Having this details in mind, the terminal impedance for the both hybrid modes corresponding to the radiating open end are given by

$$Z''_L = \frac{k_y}{w\epsilon_0}\frac{1+\Gamma''_V}{1-\Gamma''_V} \tag{1.20}$$

$$Y'_L = \frac{k_y}{w\mu_0}\frac{1+\Gamma'_I}{1-\Gamma'_I} \tag{1.21}$$

where

$$-\Gamma'_I = \Gamma'_V = (R''_{1,1})_V\Big|_{q'} = -|R''_{1,1}|e^{-j\theta}\Big|_{q'} = -|r''_{1,1}|e^{-j(\theta+\pi\gamma+\angle r''_{1,1})} \tag{1.22}$$

$$-\Gamma''_V = \Gamma''_I = (R'_{1,1})_I\Big|_{q'} = -|R'_{1,1}|e^{-j\theta}\Big|_{q'} = -|r'_{1,1}|e^{-j(\theta+\pi\gamma+\angle r'_{1,1})} \tag{1.23}$$

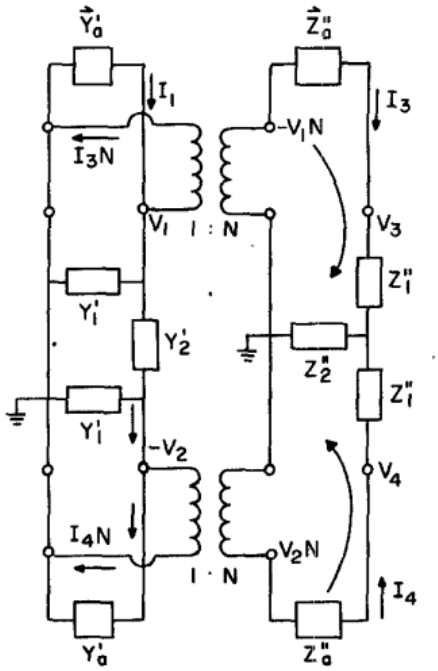

Figure 1.5: Complete network. Reproduced from [2].

Complete Transverse Equivalent Network

The last part of the analysis consist of the construction of the dispersion relation matrix, which results from the analysis via a hybrid analysis method (nodal and mesh equations) of the transverse equivalent network shown in Fig. 1.5. The dispersion relation, writing the compatibility condition for the homogeneous system of equations yields

$$\begin{vmatrix} \vec{Y}'_a + Y'_1 + Y'_2 & Y'_2 & N & 0 \\ Y'_2 & Y'_a + Y'_1 + Y'_2 & 0 & -N \\ N & 0 & \vec{Z}''_a + Z''_1 + Z''_2 & Z''_2 \\ 0 & -N & Z''_2 & Z''_a + Z''_1 + Z''_2 \end{vmatrix} \tag{1.24}$$

However, the author has noticed that there could be an error in the construction of the dispersion matrix detailed in (1.24). The sign convention

used in the transformer terminal magnitudes is found wrong when the function has been implemented as indicated in (1.24). For this reason the author propose a modification in the sign convention of the transformer terminal magnitudes. The proposal is to interpret the transformer currents in the opposite direction. With this simple modification the dispersion relation matrix becomes

$$\begin{vmatrix} \vec{Y_a'} + Y_1' + Y_2' & Y_2' & -N & 0 \\ Y_2' & Y_a' + Y_1' + Y_2' & 0 & N \\ N & 0 & \vec{Z_a''} + Z_1'' + Z_2'' & Z_2'' \\ 0 & -N & Z_2'' & Z_a'' + Z_1'' + Z_2'' \end{vmatrix} \tag{1.25}$$

and will produce the desired results.

Numerical results

Using the dispersion relation (1.25), Sanchez and Oliner[2] obtained the values of the phase constant and the leakage constant as a function of various geometric parameters. It will be shown the most relevant results obtained in this work.

For simplicity in the design, one desires that β remains constant while α varies as a function of a specific parameter. Fig.1.6(a) and Fig.1.6(b) present these dependences for a specific range of d (see Fig. 1.1).

Regarding the results of Fig.1.6(a) and Fig.1.6(b), Sanchez and Oliner have proven that a leaky-wave antenna can be readily fabricated with nonradiative dielectric (NRD) waveguide.

1.2 The development of an NRD waveguide simulator in Matlab

After having considered the theoretical basis of the NRD waveguide and how it is possible to design a leaky-wave antenna using this technology, the

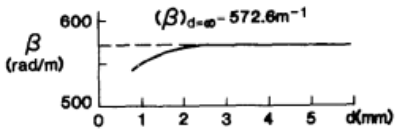

(a)

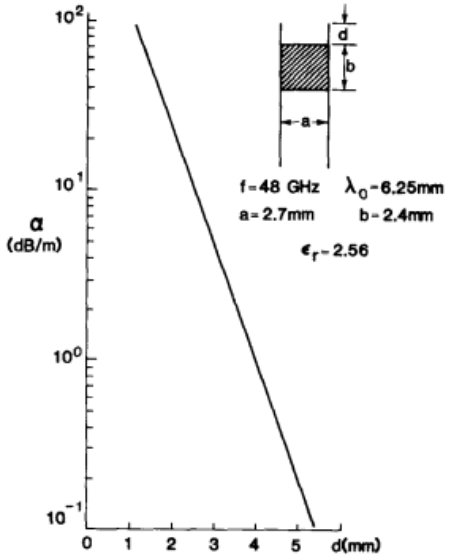

(b)

Figure 1.6: (a) Phase constant in radians/meter of the leaky-wave antenna structure as a function of d in mm. (b) Leakage constant in dB/meter of the leaky-wave structure as a function of the distance d in mm between the dielectric strip and the radiating open end. Reproduced from [2].

development of a simulator for this structure has been undertaken. The aim of this simulator is to go deep in the understanding of the structure developed by Sanchez and Oliner[2]. In addition, the software shall provide an easy and configurable tool which can be used in the future design of a similar structure using the same or other alternative technologies.

The platform used for the development of this simulator has been *Mathwork's Matlab*, an optimal platform to implement all the complex matrix and function operations required by the simulator.

The simulator has been developed in two different files. In the first file all the mathematical work operations realised in the Sanchez and Oliner paper[2] have been implemented as a Matlab function. On the other hand, just for

convenience, another file which calls the previous function and presents the results obtained has also been implemented.

The implementation of the theoretical equations into a Matlab function

As it has been explained before, the first of the files designed in the simulator is focused on the implementation of the NRD waveguide theoretical equations. The file is called $nrd\_leaky\_function.m$ and it is included as part of this work.

The complete code is detailed in the Appendix A, however, in this section the more relevant issues will be explained.

The code starts with the definitions of the global variables used, with the purpose of sharing them among the two main functions. Subsequently, the physical constants and the design variables are defined. After the definitions, the impedances and admitances of the LSE and LSM modes are implemented, both in the dielectric region and in the air region; these definitions have been taken from the Appendix of the Sanchez and Oliner paper[2]. After that, the transformer coupling factor N of the equivalent circuit, which models the coupling among the hybrid modes in the air-dielectric interface, is defined (see Fig 1.3).

Once the factors for the dielectric region, the air region and the dielectric-air interface are defined, the part of the code that describes the radiating open end is programmed. This part is substantially more delicate than the previous part because several equations are complex and are multievaluated.

In the analysis carried out by Sanchez and Oliner[2], they use the Weinstein's rigorous analysis[14] applied to TM an TE modes normally incident on the open end of parallel-plate guide, adapted to its structure. In the code developed, these equations are implemented having on mind the multiples valid values of these expressions. Particularly, following Fig. 1.4, the value of γ is forced to be negative and complex. As result of this, the value of $r'_{1,1}$ and $r''_{1,1}$ must also be forced to lay in its corresponding quadrant (see Fig. 1.4).

After this, the code implements the theoretical equations as Sec. 1.1

describes.

The implementation of a code to present the data obtained

The implementation of this code has the aim of calling the code explained before in section 1.2 in order to interpret and present the results obtained. The file which contains this code is called $nrd\_leaky\_function\_main.m$ and it is also included as part of this work.

As in the previous section, the complete code is detailed in Appendix B.

The main goal of the code developed is to obtain the propagation constant of the leaky-wave antenna γ from the simulator, introducing a variation of the distance d (see Fig. 1.1) which will cause the leakage phenomenon.

The function programmed in the previous section works as follows: for a value of γ given, the function gives the result of the dispersion relation determinant (see equation (1.25)). When the determinant is equal to zero, the value of gamma is a physical solution for a wave propagating in the structure. Therefore, the way to proceed for obtaining valid values of γ is to search for the complex roots of the determinant described in (1.25). The complex roots of this determinant will be the physical solutions of γ.

Because it is not one of the goals of this work to create a code to search the complex roots of a given function, this code has been obtained from the $FileExchange$ of $MathWorks$. The function is called $cxroot.m$[16]. This function gives the complex root of a given function, starting from an initial point which should be close to the sought for root.

As an initial point close to the root is needed for the calculation and this initial point will be complex for a radiating structure, it is very difficult to have a prior knowledge of this value. Is for this reason that it will be used an iterative algorithm in which the γ result of the previous iteration will be the initial point of the next one. The algorithm will start with a value of the parameter d big enough to make the structure not radiative. The value of gamma for this structure is easy to be calculated, because of its not-complex nature.

Once the value of γ for this conditions is calculated, the value of the pa-

rameter d will be slowly decreased in order to force the leakage phenomenon, using in each iteration the previous γ value as initial point for the next step.

Having the operation of the algorithm in mind, the development of the code is straightforward. The code defines in first place several global variables, configures different parameters such as the work frequency, and defines also a vector with all the d values. Furthermore, through a *for* loop, the iterative algorithm begins. In the last part of the code, the results are handled and shown to the user.

1.3 Results of the simulations

Once the simulator has been developed, it has been obtained the results of the different values of γ (β and α separately) in order to be compared with the results of the paper studied [2].

The results obtained shows a pretty accurate matching with the data reported in the paper. It can be appreciated a slight mismatch in the value of α which it is assumed to be due to the way we have interpreted the Weinstein's equations[14] of the radiating open end (see section 1.2).

Note that the results presented have been taken for the LSM mode. In the same way, these results can be obtained for the LSE mode of the SINRD just using the next root of the dispersion relation function.

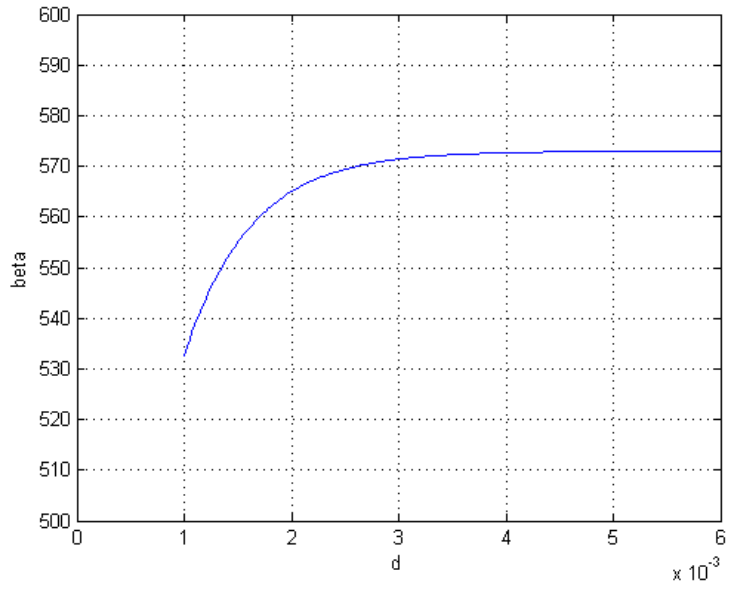

Figure 1.7: Phase constant β in radians/meter of the leaky-wave structure as a function of d in mm.

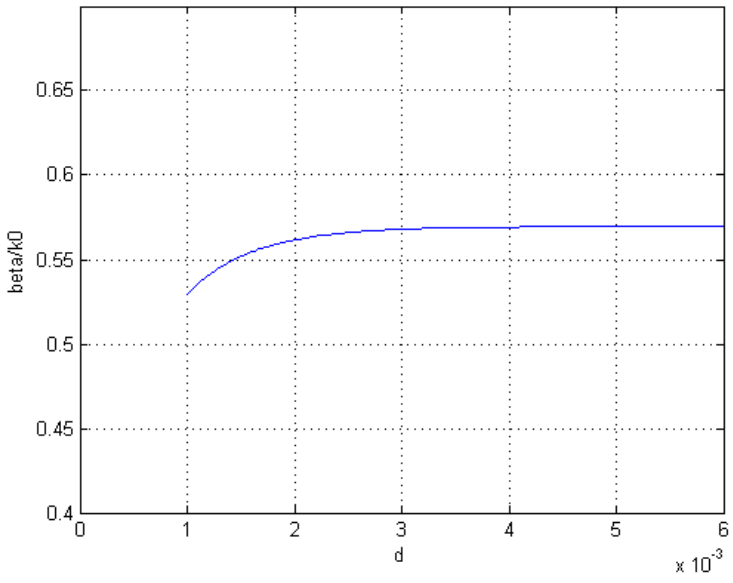

Figure 1.8: Phase constant β normalized by k_0 of the leaky-wave structure as a function of d in mm.

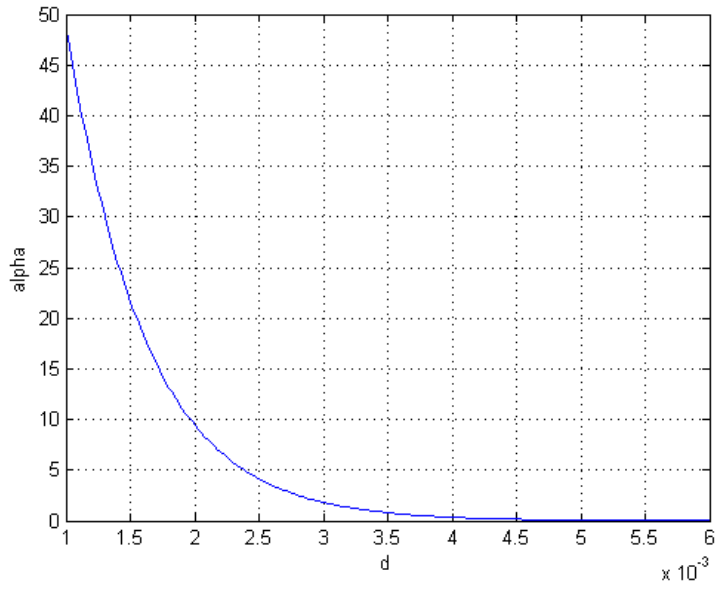

Figure 1.9: Leakage constant α in neper/meter of the leaky-wave structure as a function of d in mm.

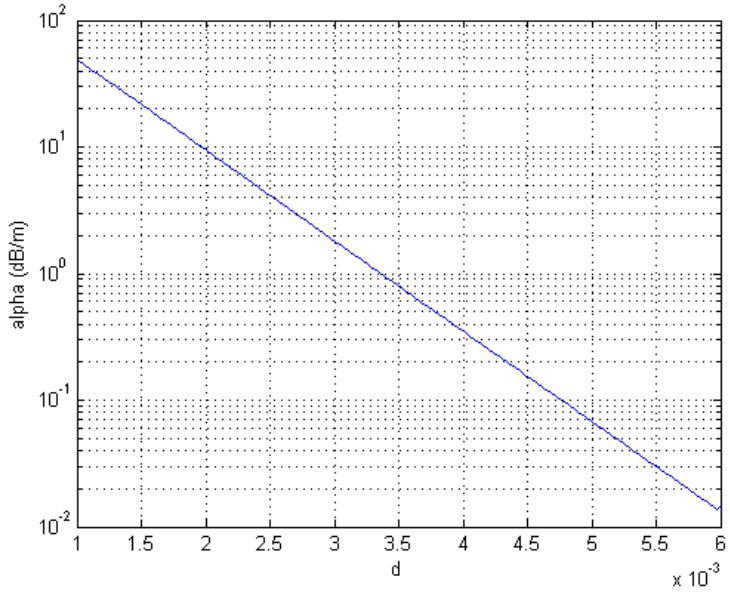

Figure 1.10: Leakage constant α in dB/meter of the leaky-wave structure as a function of d in mm.

Chapter 2

The SINRD: Study of the NRD waveguide integration into a planar structure

This chapter has, in the first place, the aim of explaining the details of the Substrate Integrated NRD (SINRD) waveguide, which represents the adaptation into planar technology of the NRD waveguide described in the previous chapter. Once the SINRD guide is explained, it will be detailed how the structure studied in Chapter 1 can be adapted to this planar technology. In addition, the advantages and problems related to this adaptation will be discussed.

2.1 The structure of the SINRD waveguide

Since the nonradiative dielectric (NRD) waveguide was proposed in [9] a large amount of papers have discussed about the implementation of this technology into millimeter-wave applications. However, it is not easy because of their mechanical tolerance and integration issues with planar circuits and active devices. Moreover, it will become more and more difficult when the operating frequency increases. This is because tolerance in the vertical (Y) direction (see Fig 2.1) related to the substrate thickness and also potential air gaps caused by mechanical assembly are much more pronounced when

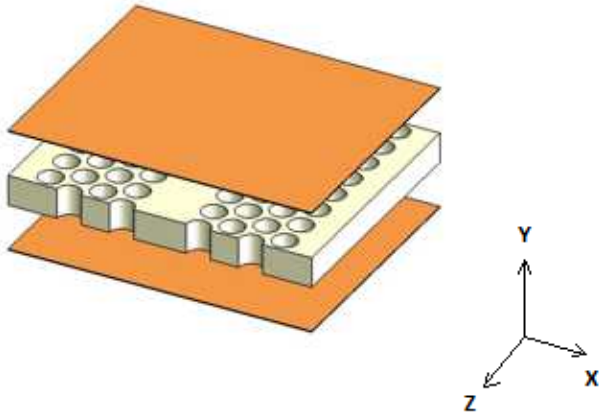

Figure 2.1: Structure of the Substrate Integrated Nonradiative Dielectric(SINRD) waveguide.

the wavelength becomes shorter.

Several attempts have been made to use substrate integration schemes to develop NRD waveguides in their planar versions. As result of these attemps the substrate integrated nonradiative dielectric (SINRD) waveguides have been successfully demonstrated [17],[18]. The structure of a SINRD is represented in Fig. 2.1. In most of the cases, special efforts were made to realize an NRD waveguide in an integrated format within a dielectric substrate by drilling an array of air holes. Those air holes can effectively reduce the permittivity of the bilateral surrounding areas of a central region, which can be controlled through the geometrical parameters of the pattern, thus creating a waveguiding dielectric channel in the substrate. Since the patterned area forms a self-supporting structure, the difficulty found in the NRD with the alignment problems is completely solved. However, since the SINRD guide needs the cover of conductors as a normal NRD guide, the potential air gaps caused by mechanical assembly also exist.

2.2 Model used to implement the air holes array

It can be affirmed that the implementation of the air holes array is the most important step in the NRD to SINRD adaptation. This air holes zones and their influence on the guided electric fields can be studied from several points of view. Using the theory explained in Chapter 1, a reflection coefficient can be defined in the transition area from the substrate to the air-holes region in order to obtain the propagation constant γ of the structure. However, as the incidence of the guided wave with the holes is oblique in both planes E and H (XY and XZ, see Fig 2.1), this study would require of complex calculation tools which would lead to develop an entire work about this topic. As this is not the aim of this work, the authors have chosen a more straightforward approximation which has been proved valid in several works [17],[19],[20]. Nevertheless the authors keep thinking that the reflection coefficient approximation would be more accurate and a interesting future line of this work.

The approximation used to study the air holes zone, is to interpret this zone as a homogeneous material region composed of a dielectric material with a lower effective relative dielectric permittivity than the relative permittivity of the material used to implement the structure. The more air volume in the structure, the lower relative permittivity of this effective material. In this way, the study presented in Chapter 1 would be completely valid with this approximation, by only modifying the relative permittivity of the air zone ($\epsilon_r = 1$) with the relative permittivity of the effective material.

The process to relate the dimensions of the holes with the relative permittivity of the effective material is also straightforward. The air holes array must be divided into cells of the same dimension. These cells will have a certain percentage of material volume and the rest of air volume (see Fig 2.2). Following the work developed by Cassivi and Wu [18] and relating the corresponding surfaces defining each region by

$$\epsilon_{eff} = \frac{\epsilon_r(S_{cell} - S_{air}) + S_{air}}{S_{cell}} \tag{2.1}$$

where S_{cell} is the surface of the cell taken, S_{air} the air surface of the cell taken and ϵ_r the relative permittivity of the material used. Having into account that for a simple holes scheme $S_{air} = \pi R^2$ and $S_{cell} = L_{cell}^2$, where L_{cell} is the lateral size of the cell, the relative permittivity of the effective material can

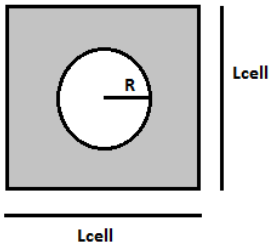

Figure 2.2: Structure of a unit cell for the hole filling region.

be obtained simply by

$$\epsilon_{eff} = \frac{\epsilon_r(L_{cell}^2 - \pi R^2) + \pi R^2}{L_{cell}^2} \tag{2.2}$$

The holes array schemes can be several, depending on the effective permittivity to achieve. Some works use a scheme based on two holes of different radii [17], while others use a scheme based on rectangular holes [4]. However in this work it will be used a simple scheme based on a circular hole [19],[20], because of its implementation simplicity and its capability to obtain the required relative effective permittivity.

2.3 Influence of the Relative Effective Permittivity into a SINRD waveguide

Qualitative analysis based on Ray Theory

As has been explained, the different ratio of air/dielectric area can be directly related with a certain relative effective permittivity. Therefore, this permittivity becomes an important electrical parameter for the design of a SINRD structure.

The effective permittivity value of the holes region will affect strongly the value of the phase constant β and, in a lesser degree, the value of the leakage constant α.

In order to have a first idea of how the phase constant β will vary with the effective permittivity of the holes zone, the structure can be studied from the ray theory point of view used mostly in high frequency systems such as the optical fiber. This simplified analysis interprets the propagative wave as a ray, and studies its behaviour through the Snell's law. Although this study will not find the exact wave parameters of the propagation, it will indicate the right tendency.

Considering the structure as an internal region with a certain refractive index where the ray will be propagative, and an external zone with a lower refractive index where the ray will be reflected under certain conditions, the ray model and the Snell's law can be used.

Under these considerations and using the ray model [21], the Snell's law equation establishes the following relations:

$$\frac{\sin\theta_1}{\sin\theta_2} = \frac{n_2}{n_1} \tag{2.3}$$

$$\sin\theta_1 = \frac{n_2}{n_1}\sin\theta_2 \tag{2.4}$$

where the critical angle θ_{crit} is the value of θ_1 for which θ_2 equals 90°:

$$\theta_{crit} = \arcsin(\frac{n_2}{n_1}\sin\theta_2) \tag{2.5}$$

$$\theta_{crit} = \arcsin\frac{n_2}{n_1} \tag{2.6}$$

Taking into consideration that the desired region where the SINRD has to operate is placed below the critical angle (because this is the region in which the guiding process occurs by the proximity of the parallel plates), it can be affirmed that as the permittivity of the hole zones is increased, the maximum operating frequency will be increased.

In order to know the minimum operation frequency it will be necessary to perform a more complex analysis.

Results obtained with the simulator designed

In order to confirm the expect trend, a modification of the simulation code implemented in Chapter 1 was developed. In this simulations the working frequency and the effective permittivity of the holes zone have been taken as variables, and the simulator calculates, as usual, the parameters α and β. The parallel plate air region in the original structure ($\epsilon_r = 1$), is now replaced by an effective medium of relative dielectric constant ϵ_{eff}, calculated with equation (2.2).

Note that the results presented have been taken from the LSM mode, the same mode used in the results shown in Chapter 1. In the same way, these results can be obtained for the LSE mode of the SINRD.

The codes are included as part of this work in the files *sinrd_leaky_beta_er.m* and *sinrd_aprox_function.m*.

The results are detailed in the figures 2.3 and 2.4. As it can be observed, the variation of the effective permittivity affects the phase constant in a stronger way, showing almost unchanged zones in the leakage constant figure. This fact could be used in a future to implement certain illumination profile in the antenna. However, at this point it serves to design the appropriate holes pattern of the SINRD.

Analysis of the structure performance depending on the working frequency

The next important step in the design of any microwave component is the frequency response. The frequency response of the device will be determined by the cutoff frequency and by its bandwidth.

In order to calculate these parameters, it has been modified the simulation tool to introduce the operational frequency as a variable. In this way, the structure can be analysed over a huge range of frequencies. The code is included as part of this work in the file *sinrd_beta_frec.m*.

In the same way as it has been done so far, the results presented are for the LSM mode of the SINRD. It is important to notice that the interesting

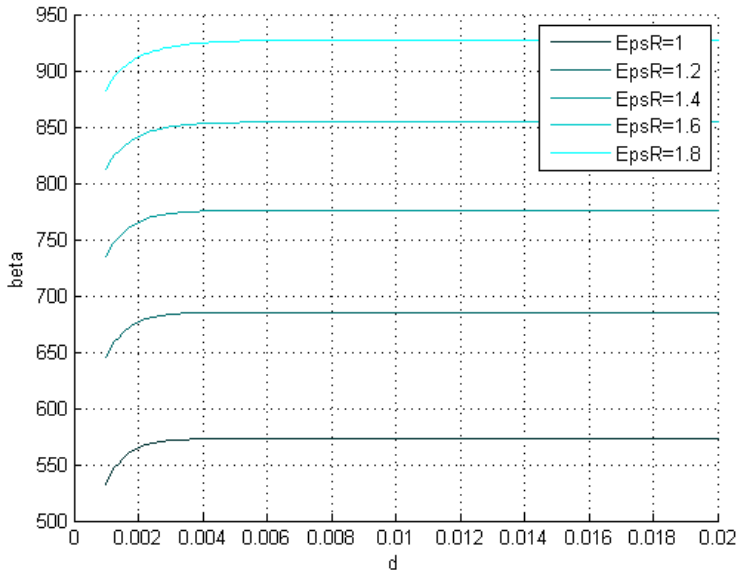

Figure 2.3: Variation of the phase constant controlling the d (see Fig. 1.1) and ϵ_r of the hole zones parameters.

bandwidth of the structure will include the frequency range from the cutoff to the frequency value in which the wave becomes a $slow - wave$, which occurs when the relation $\beta/k_{holes} > 1$ is satisfied [1]. In the $slow - wave$ range, the energy is not guided because of the NRD principle. In this range the guiding mechanism of the wave in the central zone is not due to the proximity of the parallel plates. On the contrary, the guiding mechanism is because of the refraction index difference among the central zone and the *attenuation* zone (as in the optical fiber). It is also for this reason, that the simulator could give wrong results out of this range.

Note that in this region the parallel plates will not be able to control the radiation properties of the mode, as the wave suffers total reflection on the interface between the dielectric and the air-hole zone.

The bandwidth for different values of the dielectric constant of the holes zone can be viewed in the figures 2.5, 2.6, 2.7 and 2.8. From the results it can be concluded that as the dielectric constant of the holes region increases, the cutoff frequency decreases, and the bandwidth becomes larger.

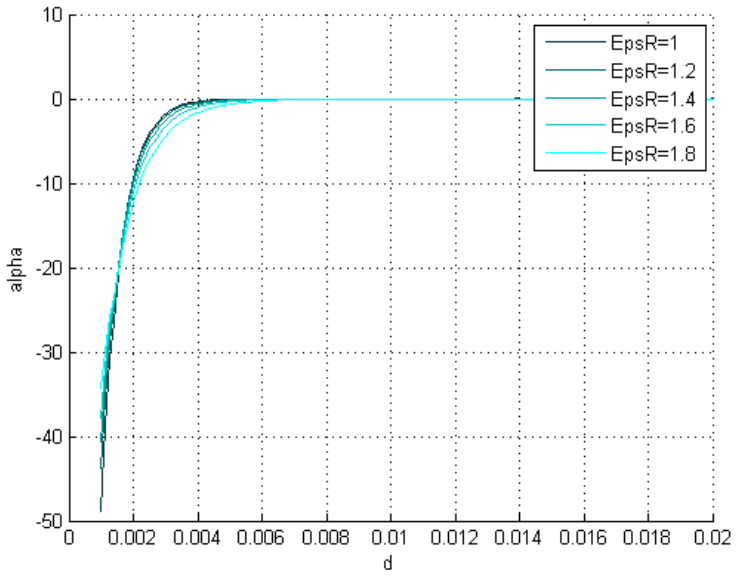

Figure 2.4: Variation of the leakage constant controlling the d (see Fig. 1.1) and ϵ_r of the hole zones parameters.

2.4 The problematic of the modes excitation in the SINRD structure

In this section it is described the problem of the modes excitation of the SINRD, and also in the original NRD structure. This is, from the point of view of the author, the main disadvantage when designing a system based on this technology. As a consequence, several scientific works have tried to find a proper solution to the mentioned problem[3].

In Chapter 1 the presence of the hybrid modes LSE and LSM has been discussed. These modes present the field distributions shown in Figure 2.9. The field patterns make difficult their excitation with the traditional feeding circuits (coaxial, microstrip, rectangular waveguide...). In addition, it is usually necessary to excite only one of the hybrid modes and at the same time to not excite the other.

A procedure to feed the structure through a microstrip line while being able to excite each mode separately has been developed by Bacha and Wu in [3]. The structure is shown in Fig. 2.10. In that paper the microstrip to

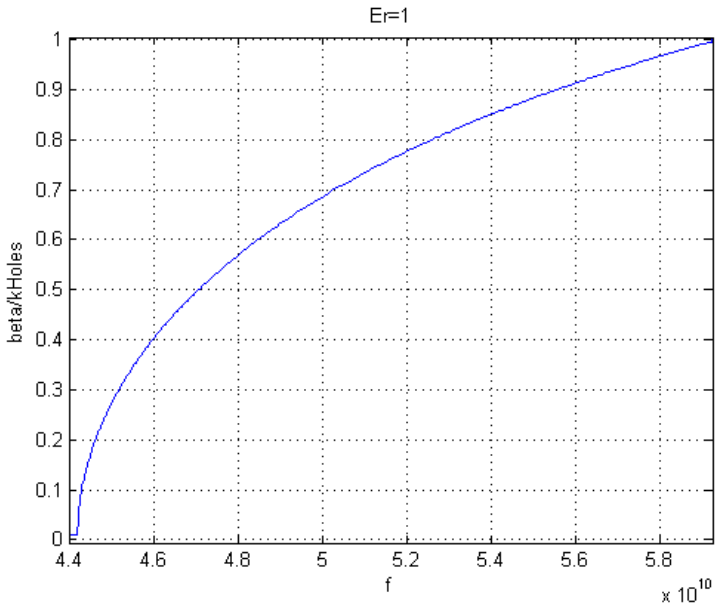

Figure 2.5: β/k_{holes} as a function of the frequency in the SINRD structure for an ideal $\epsilon_{holes} = 1$.

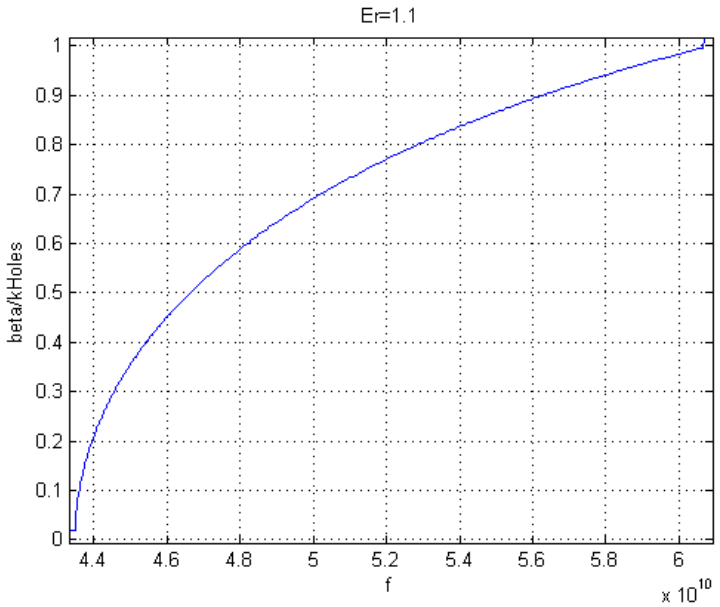

Figure 2.6: β/k_{holes} as a function of the frequency in the SINRD structure for an $\epsilon_{holes} = 1.1$.

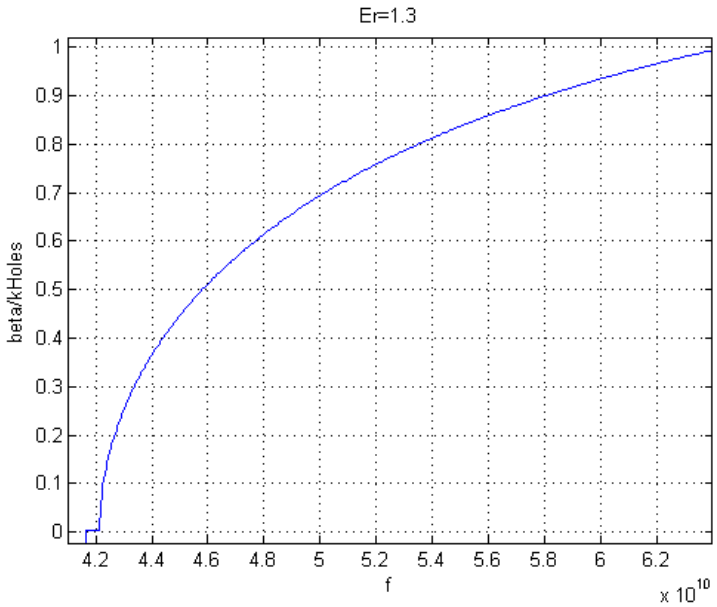

Figure 2.7: β/k_{holes} as a function of the frequency in the SINRD structure for an $\epsilon_{holes} = 1.3$.

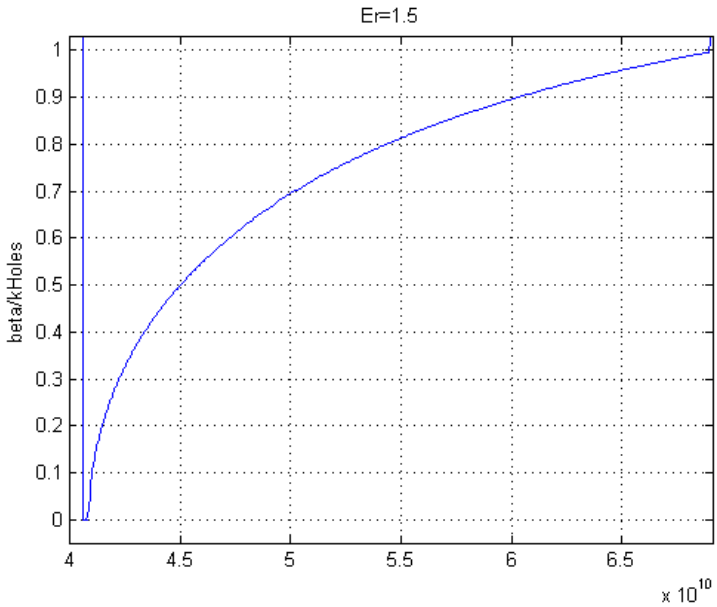

Figure 2.8: β/k_{holes} as a function of the frequency in the SINRD structure for an $\epsilon_{holes} = 1.5$.

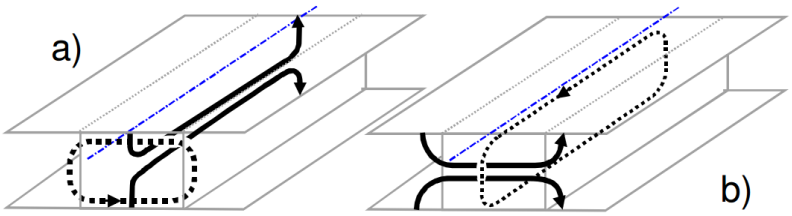

Figure 2.9: Structure of an NRD guide and field distributions of the fundamental modes (solid line: electric field, dotted line: magnetic field; (a) LSE mode (b) LSM mode).

NRD coupling is made through an horizontal or vertical slot depending on the excited mode. This is a solution easy to manufacture but it exhibits a narrow bandwidth and some losses due to the coupling slot.

Another way to excite the NRD circuits, this time through a rectangular waveguide, was developed by Xu and Wu in [4]. The structure is shown in Fig. 2.11. In this rectangular waveguide to SINRD transition it is used a tapering both in the E and H plane of the rectangular waveguide. This solution provides a good performance, however, it also requires complex manufacturing process.

As it has been explained, it does not exist a solution involving planar structures, good performance and simple fabrication process, when the feeding circuit of a NRD or SINRD has to be designed. It is for this reason that this problem has to be taken into account when the fabrication of a SINRD circuit is planned, choosing the best possible solution.

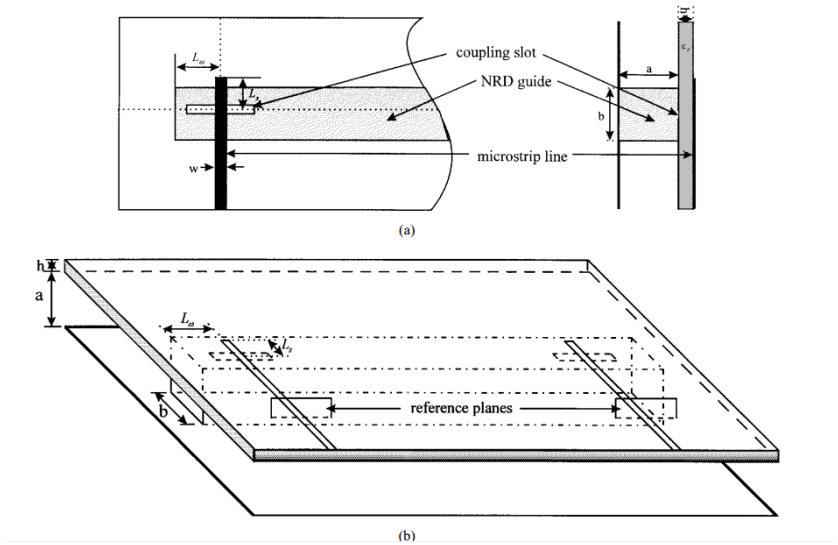

Figure 2.10: Microstrip to NRD transition proposed by Bacha and Wu, seen from above(a), circuit setup(b). Reproduced from [3].

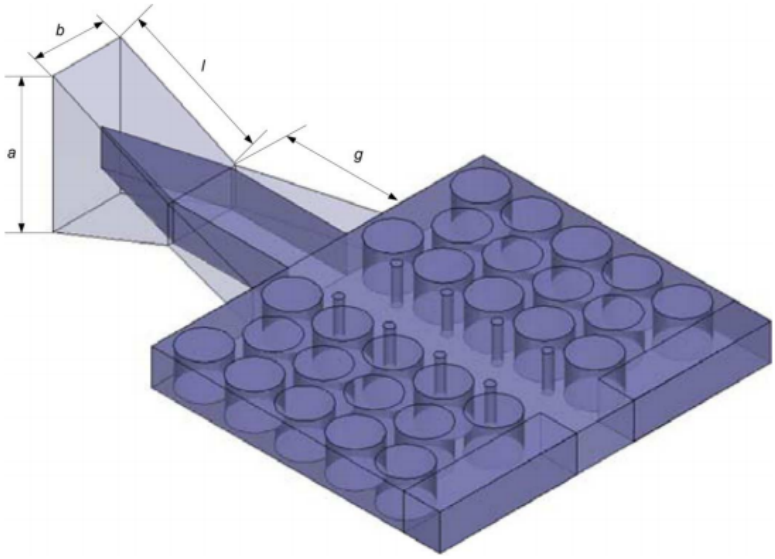

Figure 2.11: WR19 rectangular waveguide to SINRD transition proposed by XU and Wu. Reproduced from [4].

Chapter 3

Design of a SINRD leaky-wave antenna at 20 GHz

The present chapter is aimed to illustrate the design process of a leaky-wave antenna based on the Substrate Integrated Non-Radiative Dielectric technology. This antenna is achieved by shortening the lateral dimension of the SINRD waveguide (as in the NRD leaky-antenna, see Fig. 1.1). The theoretical basis of this phenomenon is explained in Chapter 1 of the present work.

The design process is composed of two stages. In the first one, a theoretical study based on the NRD modelling equations (detailed in Chapter 1 Section 1.1) and the simulation tool created with Matlab, is carried out. At the end of this stage the values of the parameters β and α and their dependence with the design parameters will be obtained.

In the second stage a more practical study based on the commercial software package *Ansys HFSS* is realised. Through this software tool, a physical layout of the circuit is designed and simulated. At the end of this stage the Scattering parameters of the leaky-wave antenna, as well as the β and α parameters, will be obtained. These results will be compared against the ones obtained by the theoretical equations. Therefore, the design process scheme can be described as follows:

1. Select the working frequency, the dielectric constant of the employed

material and the dielectric constant desired in the holes zone. Also select the dimensions a and b (see Fig. 3.1). The parameter a has to be less than half a wavelength to work as a Non Radiative Dielectric waveguide. Explanation about this selection can be found in Chapter 1 Sec. 1.1.

2. Theoretical stage

   (a) Obtain the β parameter for a non-leaky structure. This can be done by selecting a value of d (see Fig. 3.1) large enough to be considered as infinite. Under this situation compute the propagation constant for both the LSE and LSM modes.

   (b) Model the leaky radiation reducing the distance d, measuring the value of β and α when this distance is decreased. The procedure is detailed in Chapter 1 Sec. 1.1.

   (c) Obtain the variation of β with different values of the holes zone dielectric constant. Obtain β for the frequency range where the propagation is fast-wave.

3. Layout stage

   (a) First design of the simplified structure. Design of the non-leaky waveguide modeling the holes region as a homogeneous material with the same effective dielectric constant. Obtain the S parameters and the β value with the HFSS full-wave electromagnetic simulator.

   (b) Introduce to the previous design the leakage phenomenon decreasing the distance d. Obtain the dependence of β and α with d with the HFSS full-wave electromagnetic simulator and compare them with the theoretical results.

   (c) Final design of the complete structure. Design of the non-leaky waveguide with the real holes. Obtain the Scattering parameters and the β value with the HFSS full-wave electromagnetic simulator.

   (d) Introduce the leakage phenomenon to the previous design decreasing the distance d. Obtain the dependence of β and α with d with the HFSS full-wave electromagnetic simulator and compare them with the theoretical results. Obtain also the radiation patterns.

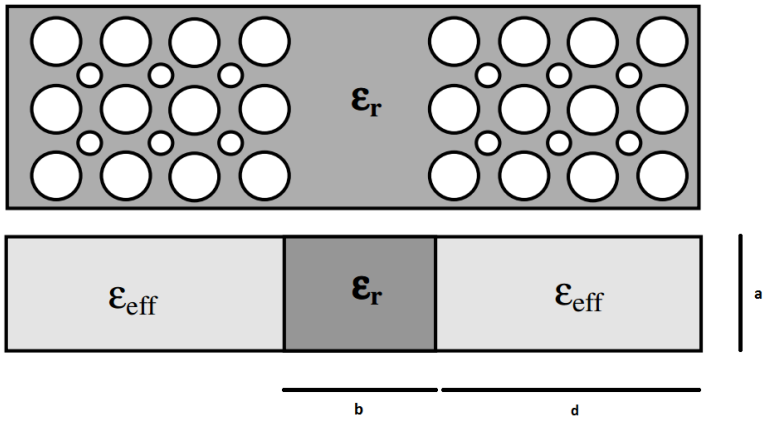

Figure 3.1: SINRD dimensions.

3.1 Design requirements applied to a 20 GHz antenna

The design of this antenna has been made to fulfill the requirements of materials, devices and resources available in the microwave laboratory at the *Università degli studi di Pavia*. The main purpose was to select a proper design capable of being built and measured in this laboratory, therefore, the design variables are restricted as follows:

- The working frequency upper limit has been selected to be about 25 GHz, this is because of the available measurement equipment, the difficulties in the construction of high frequency circuits and the thickness of the materials available.
- The thickest dielectric material available is the Taconic CER-10 which has a dielectric constant of 10 and a thickness of 1.27 mm.
- The diameter of the holes has to be in the range 0.2-2 mm because of the milling/drilling machine restrictions.
- The minimum possible effective dielectric constant of the holes region is about 5 (see equation 2.2). This value could be decreased if a more complex pattern for the holes were selected.

Having all these requirements in mind and also knowing that it exists a compromise between working frequency and thickness, this is, the higher the thickness, the lower the working frequency, the design parameters have been configured as follows:

- $a = 2.54mm$ (see Fig. 3.1).
- $b = 7.62mm$ (See Fig. 3.1).
- Selected material dielectric: Taconic CER-10. $\epsilon_r = 10$. $tan\delta = 0.0035$.
- Working frequency=20 GHz.
- Radius of the holes=1mm.

Notice that the a parameter value (see Fig. 3.1) is the double of the material thickness. This problem could be solved by using a construction scheme based on two stacked dielectric layers.

3.2 Theoretical stage for the design of a 20 GHz antenna

Obtaining β for both LSE and LSM modes in a non-leaky structure

Once the design parameters are defined, the first step is to obtain the value of β for both LSE and LSM modes. At the same time, it is also necessary to know if these modes are propagative over the non-leaky structure.

Using the simulator designed and explained in Chapter 1, the theoretical equations for an scenario given (see eq. 1.25) are solved, finding the values of β which makes valid the dispersion equation[2] of the structure. Equation (1.25) represents the transverse resonance equation of the structure under analysis. The values of β that satisfy this equation correspond to valid solutions, therefore giving the phase constant for the physical modes that can propagate in the structure. Figure 3.2 shows the values of β that satisfy this equation.

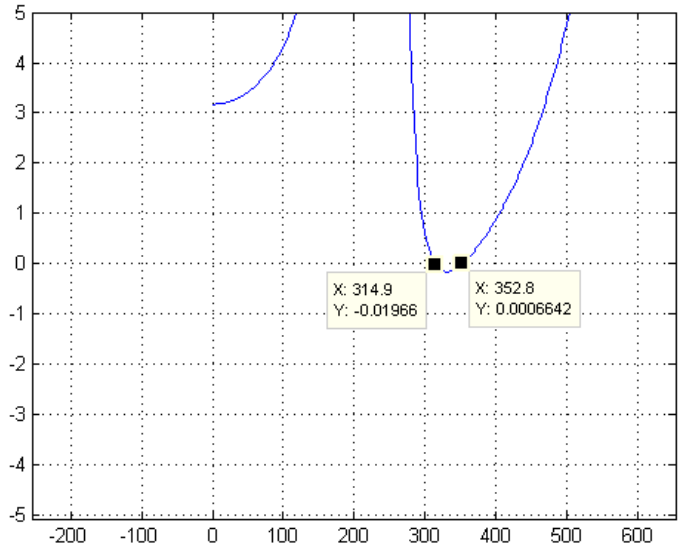

Figure 3.2: Results of the dispersion equation for different values of β.

In an NRD structure the lower hybrid mode is the LSE [22]. Therefore when both modes LSE and LSM are present in the structure, the one with higher value of β will be the LSE and the one with the lower will be the LSM. In this way, the hybrid modes can be directly identified. Therefore, observing Figure 3.2, it can be affirmed the following:

- Value of β at 20 GHz for the LSE mode: 352.8 rad/m
- Value of β at 20 GHz for the LSM mode: 314.9 rad/m

Modeling the leaky radiation for the LSE mode

Once the modes have been identified it is necessary to know which mode will be the one used in the leaky-wave antenna. The other one will be considered as a non-desired spurious mode. It could be possible to design a structure in which the two modes could operate together because both are orthogonal to each other[23]. However, due to the limited scope of this work, the structure has been designed to work only with one mode. In any case, this could be an interesting possible future line.

The mode used in the leaky antenna designed will be the LSE mode. This is the first hybrid mode guided in the structure[22], and as consequence it presents the lowest cutoff frequency, which will help with the measurements.

In order to study the leakage for this LSE mode it has been introduced the parameter d (see Fig. 3.1) which models the lateral size of the structure. The smaller the distance d, the stronger the radiation from the structure. This is because the mode below cut-off in the hole filled region will reach the end of this region sooner, and then more energy will be radiated.

The results for the value of β and α according to the variation of d are shown in the Figures 3.3 and 3.4.

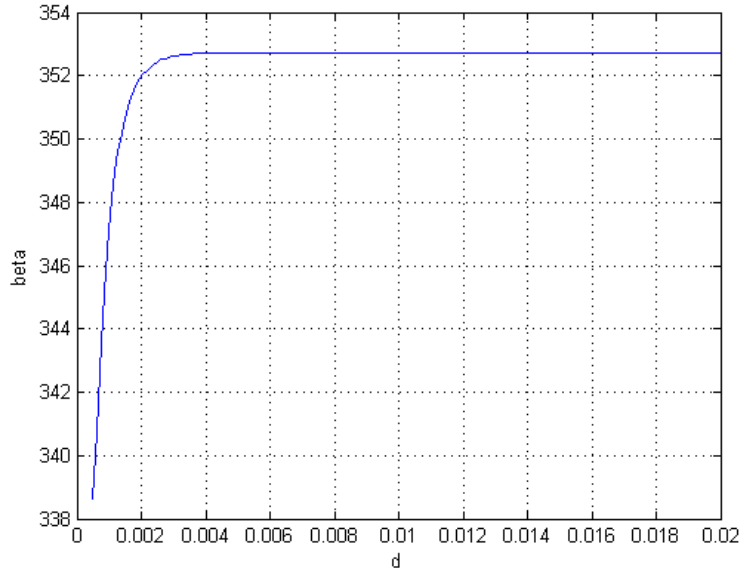

Figure 3.3: β as a function of the distance d for the considered structure. f=20 GHz. ϵ_r=10. ϵ_{rholes}=5. a=2.54mm. b=7.62mm.

Obtaining the variation of β as a function of the frequency and the effective relative permittivity of the air holes region for the LSE mode

Once the leakage losses have been detailed, a study of how some design parameters (such as the frequency and the effective relative permittivity of the air holes region) affect to the mode propagation has been performed.

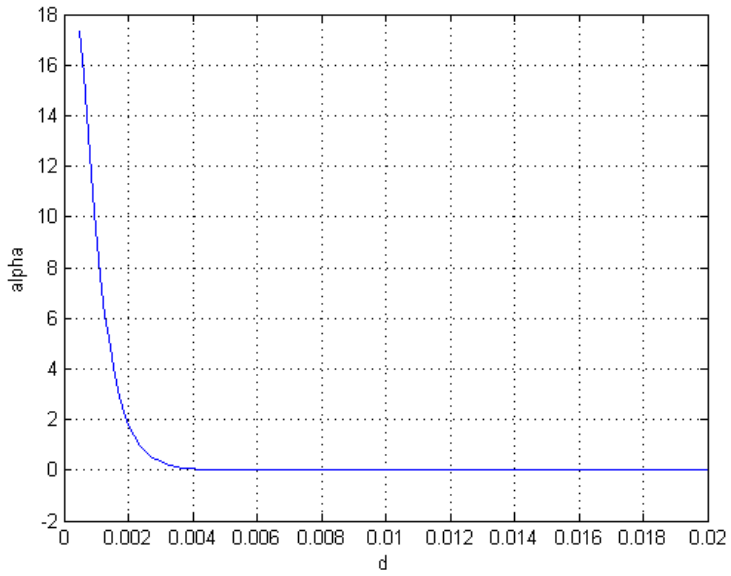

Figure 3.4: α as a function of the distance d for the considered structure. f=20 GHz. ϵ_r=10. ϵ_{rholes}=5. a=2.54mm. b=7.62mm.

In the first place, the variation of the parameters β and α depending on the ϵ_{rholes} value has been obtained. This can be observed in Figures 3.5 and 3.6.

Observing these figures, it can be affirmed that as the effective dielectric constant of the holes zone is increased, the value of β grows and the value of α is only affected in its slope. This information is crucial for modifying the design as well as for controlling the leakage parameters (such as the radiation angle, directly related with β) in more advanced stages.

To conclude this stage the frequency response and bandwidth of the circuit where the operation is fast-wave have been obtained. These results can be observed in Figure 3.7 for a non radiative structure(d=∞). As can be observed, the cutoff frequency is 19.26 GHz and the maximum radiation frequency is 27.53 GHz.

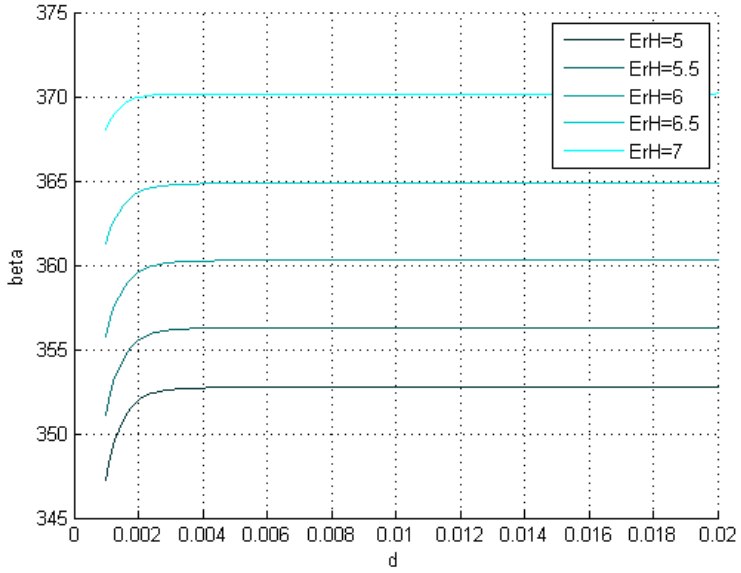

Figure 3.5: β as a function of the distance d and $\epsilon_r$holes for the considered structure. f=20 GHz. ϵ_r=10. a=2.54mm. b=7.62mm.

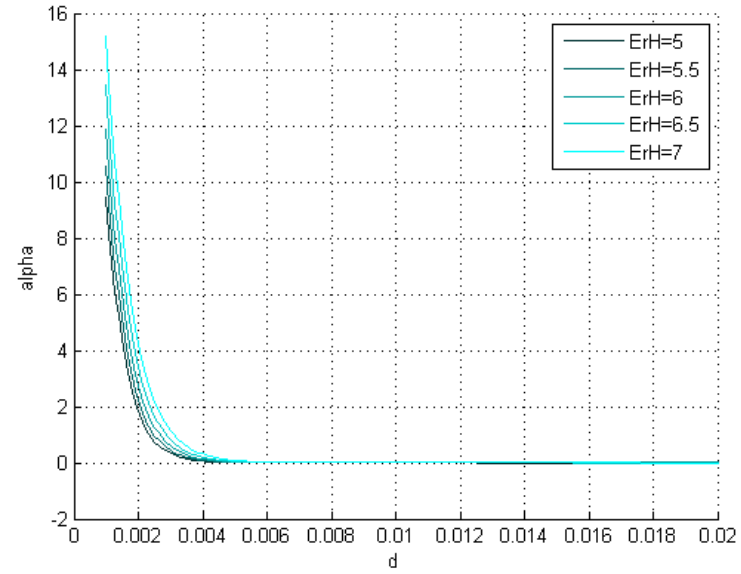

Figure 3.6: α as a function of the distance d and $\epsilon_r$holes for the considered structure. f=20 GHz. ϵ_r=10. a=2.54mm. b=7.62mm.

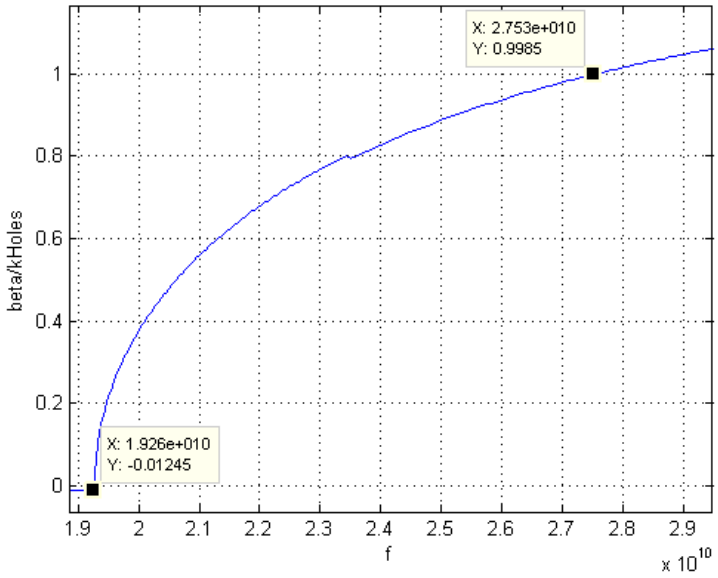

Figure 3.7: Normalized β according to the variation of the frequency for the scenario given. ϵ_r=10. $\epsilon_r$holes=5. a=2.54mm. b=7.62mm.

3.3 Layout stage for the design of a 20 GHz antenna

First design of the simplified structure

The first approximation to the final design of the antenna is to realise a simplified design of the non-leaky structure, implementing the holes zone as a uniform dielectric material with a lower dielectric constant, as compared to the dielectric constant of the substrate.

In this first design, moreover, the symmetry planes associated to the LSE mode have been used in order to reduce simulation time. Having in mind these details, the structure of Figure 3.8 has been designed and simulated with the commercial software HFSS to obtain the Scattering parameters.

Notice that the LSE mode has an H-plane symmetry (magnetic symmetry plane) in the plane YZ and another H-plane symmetry in the plane XZ (both referenced to Figure 3.8). A deeper study about the symmetry planes

presented in the hybrid modes is performed in Chapter 4. A representation of the module of the electric field in the structure can be observed in Figure 3.9.

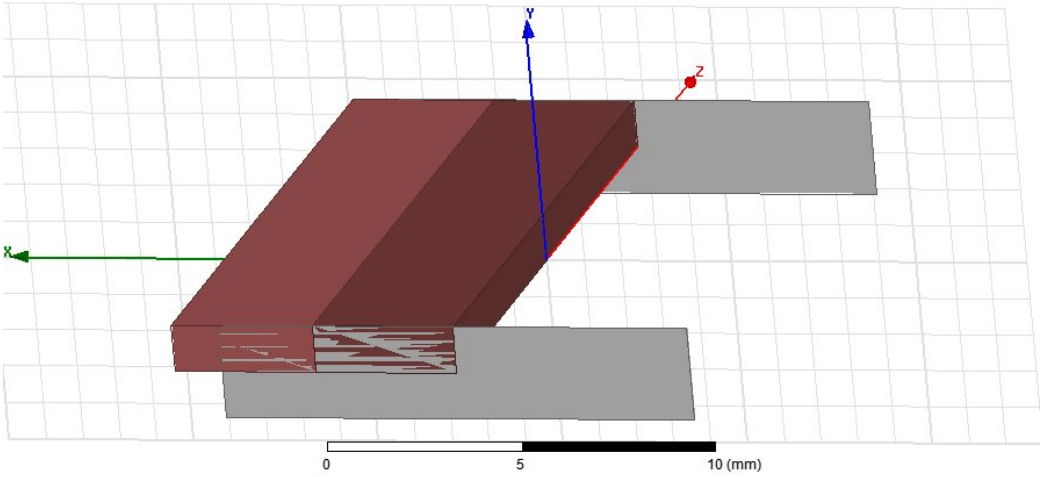

Figure 3.8: Simplified design of the non-leaky structure using the symmetry planes of the LSE mode. ϵ_r=10. $\epsilon_r$holes=5. a=2.54mm. b=7.62mm.

Once the structure has been simulated, the Scattering parameters obtained are represented in Figure 3.10. From the representation of the Scattering parameters, the cut-off frequency of the structure can be observed by a sharp increase of the reflection coefficient below the frequency 19.28 GHz. This frequency is consistent with the one obtained by the theoretical equations. On the other hand, the figure shows a typical behaviour of a wave guided through a structure with a small reflection (S_{11}) and a high transmission to the output port (S_{22}). Note that this behaviour is maintained in a large frequency bandwidth, for frequencies higher than the cut-off frequency of the structure when it operates as a leaky-wave antenna.

The parameter β obtained by HFSS can be also analysed. Figure 3.11 shows its behaviour. In this figure the value of β and the cutoff frequency can be observed, being both consistent with the theoretical results.

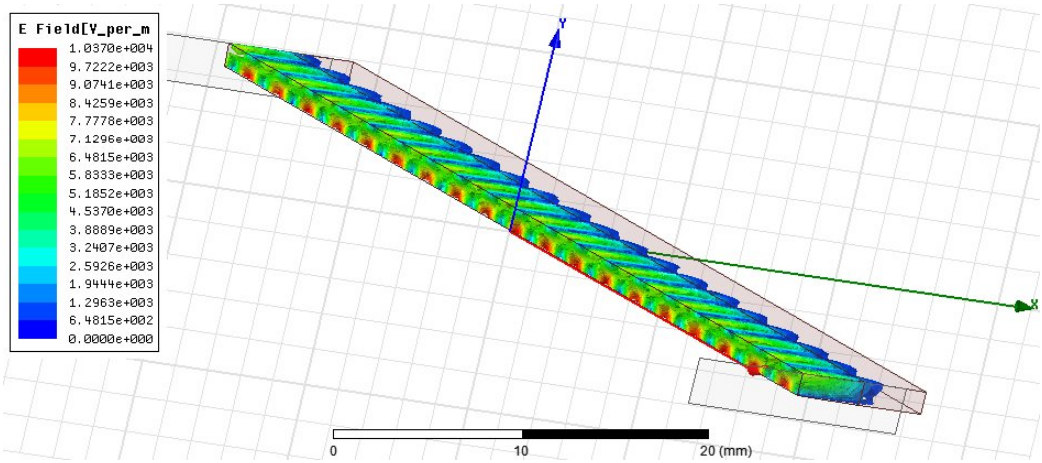

Figure 3.9: Representation of the module of the electric field in the structure of the Figure 3.8.

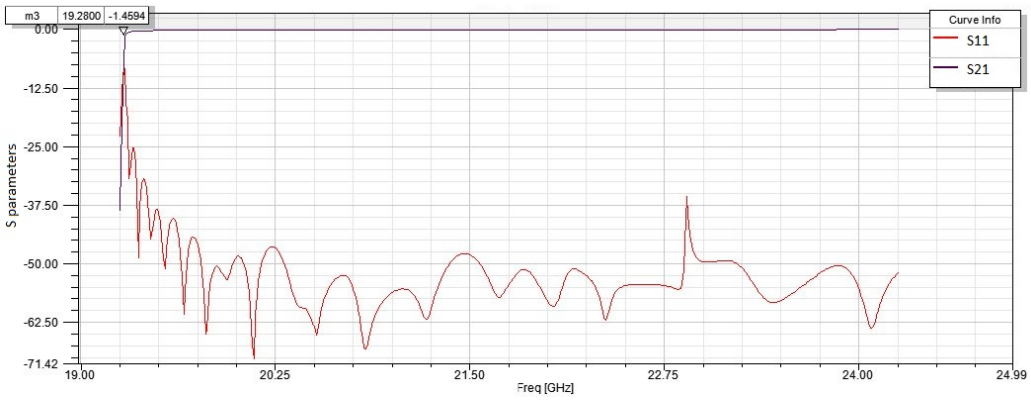

Figure 3.10: Scattering parameters obtained from the structure of the Figure 3.8, as a function of frequency

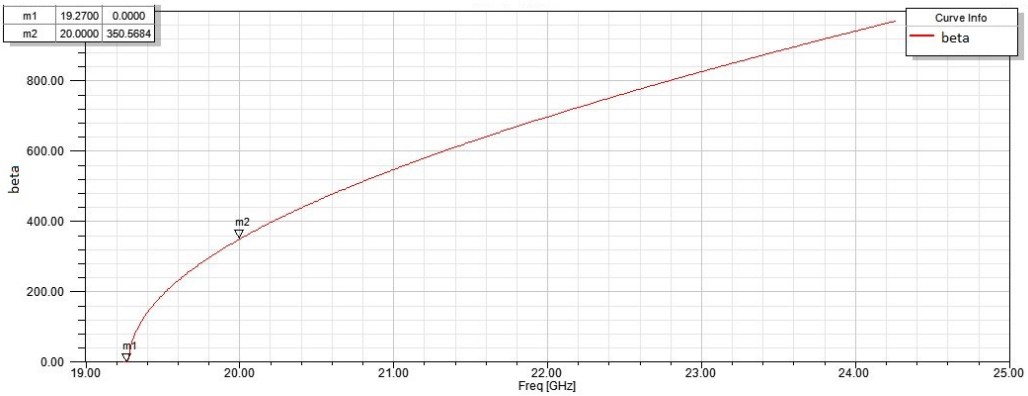

Figure 3.11: β obtained from the structure of the Figure 3.8.

Adding the leakage phenomenon to the first design of the simplified structure

Once the previous results have been justified, the next step is to introduce the leakage phenomenon in the first design. This time the vertical symmetry H-plane (plane YZ) can not be used because of the discontinuity introduced. However, the horizontal H-plane symmetry is still used in order to reduce the simulation time.

To implement this leakage phenomenon, one of the lateral faces of the structure has been designed with a variable length d. In this way, the whole structure can be studied by using a parametric analysis, as a function of this distance.

The layout can be observed in Figure 3.12, and the distribution of the module of the electric field in Figure 3.13.

At the time of studying the Scattering parameters, it is important to observe the variation of the S_{21} with different values of d. As d decreases, the leakage radiation increases, and the parameter S_{21} falls. This effect is stronger for lower frequencies because they carry more energy out of the central dielectric. This behaviour can be observed in Figure 3.14. When $d = 2mm$ the value of S_{21} at 20 GHz is about -0.7 dB, meaning that practically there is no leakage. On the other hand, when $d = 0.5mm$ the value of S_{21} at 20 GHz is about -8.02 dB, that is, more than half of the energy is radiated (the energy reflected can be considered insignificant).

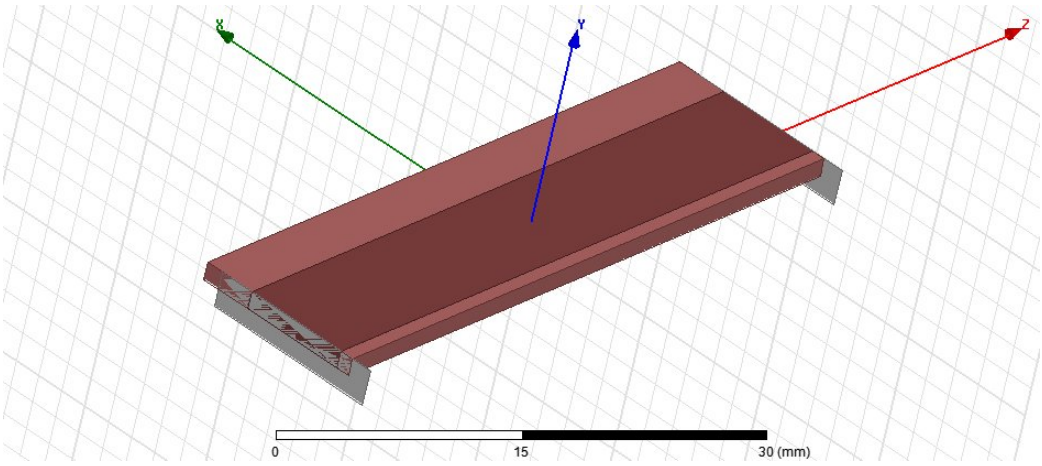

Figure 3.12: Simplified design of the leaky structure using the horizontal symmetry H-plane of the LSM mode. ϵ_r=10. $\epsilon_r$holes=5. a=2.54mm. b=7.62mm.

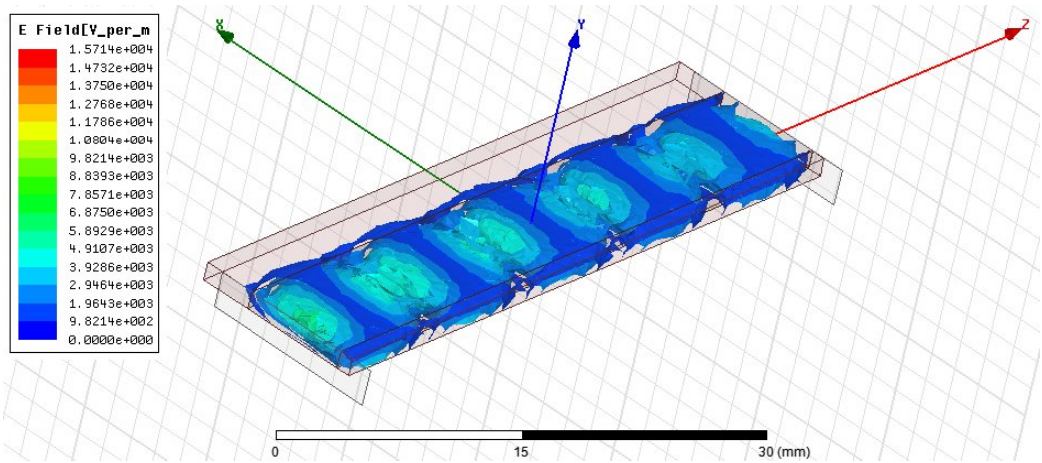

Figure 3.13: Representation of the module of the electric field in the structure of Figure 3.12.

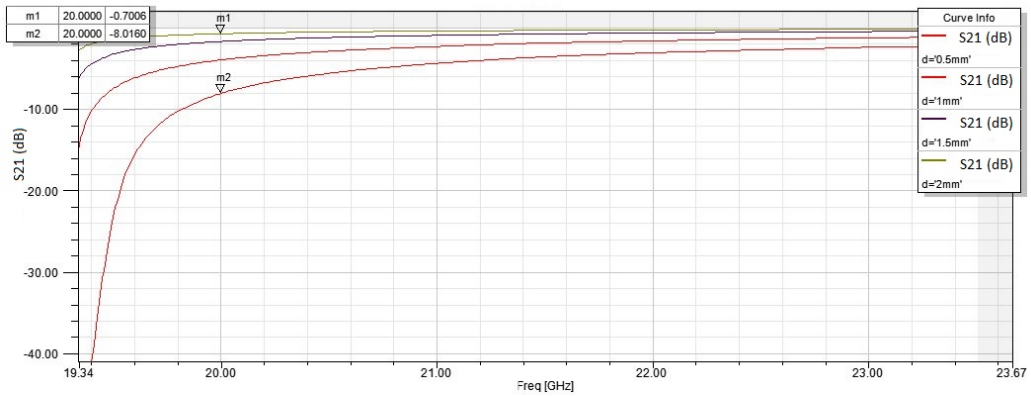

Figure 3.14: $|S_{21}|$ for the structure of the Figure 3.12 with different values of d.

Another interesting analysis could be the value of the α parameter for these different values of d. This can be observed in Figure 3.15. In this case, the α value has been calculated with the following relation from the S parameters

$$2L\alpha = -\ln \frac{|S_{21}|^2}{1-|S_{11}|^2} \tag{3.1}$$

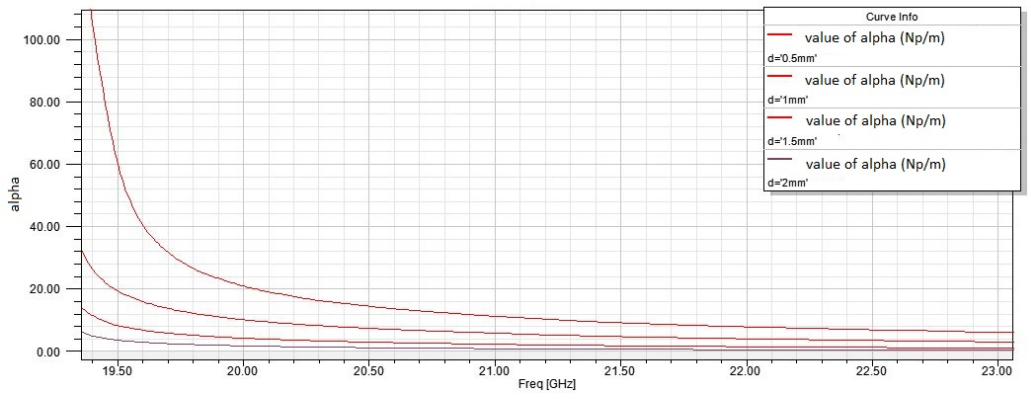

Figure 3.15: α for the structure of the Figure 3.12 with different values of d.

Final design of the non-leaky structure. Design of the non-leaky waveguide with the real holes

When the simplified structure is tested and all the results are consistent with the theory, it is time to introduce the real holes to the design in order to check how these discontinuities affect to the results obtained by the simplified model.

The structure designed is shown in Figure 3.16. In this case, the two symmetry planes compatible with the LSE mode are used again to reduce the simulation time.

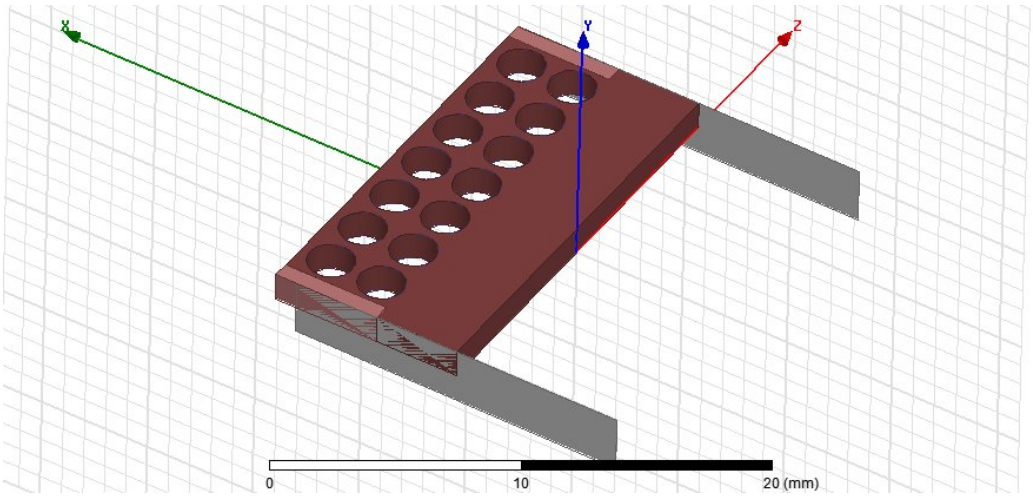

Figure 3.16: Complete design of the non-leaky structure using the symmetry planes of the LSE mode. ϵ_r=10. ϵ_{rholes}=5. a=2.54mm. b=7.62mm.

Notice that a small piece of the *fictitious* dielectric has been introduced next to the ports of the waveguide in order to reduce the reflections due to the discontinuity produced by an air hole too close to the port.

Observing the distribution of the electric field in Figure 3.17, it can be observed that the electric field remains confined inside the central part of the dielectric and it is evanescent in the holes zone as expected.

Observing also the results presented in Figure 3.18 and Figure 3.19, it can be noticed that the waveguide operates as expected and the values of β at 20 GHz and the cutoff frequency are consistent with the theory.

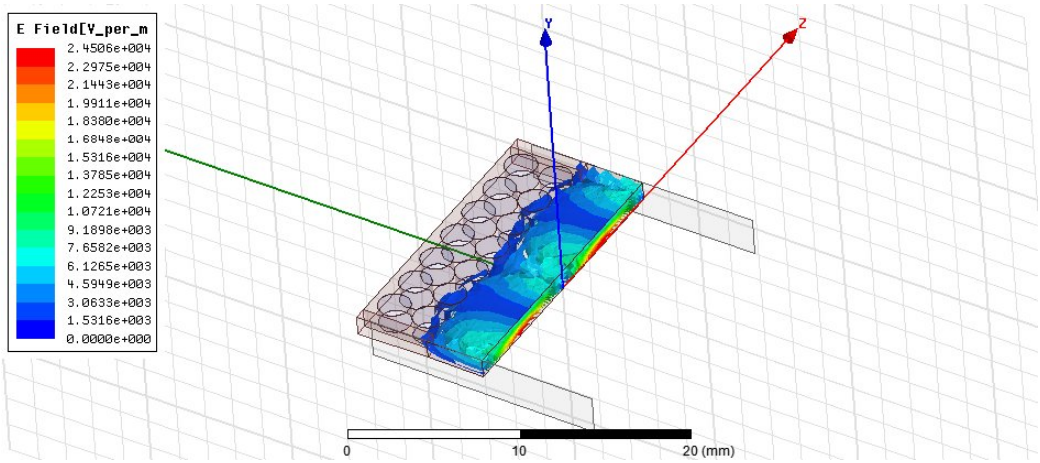

Figure 3.17: Representation of the module of the electric field in the structure of the Figure 3.16.

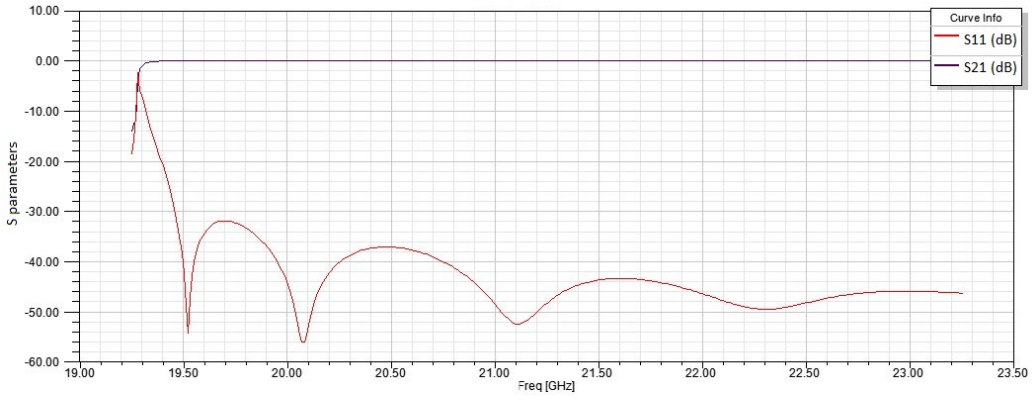

Figure 3.18: Representation of the Scattering parameters for the structure of the Figure 3.16.

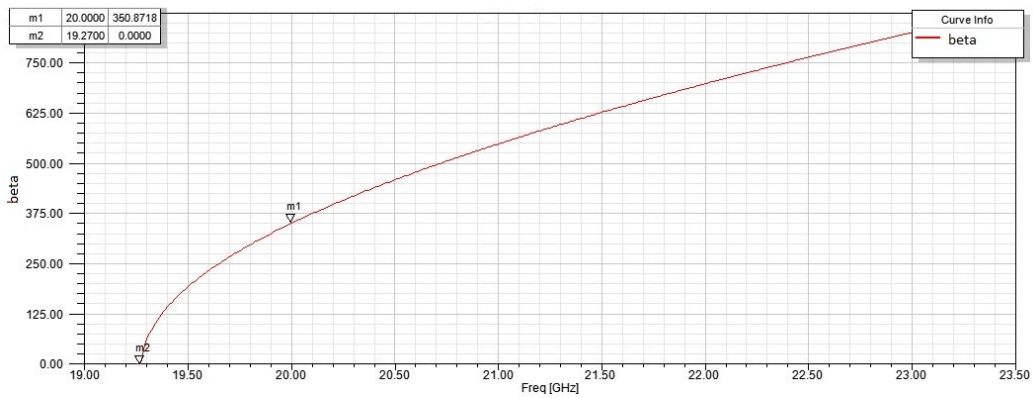

Figure 3.19: β in the structure of the Figure 3.16.

Final design of the complete structure

As the last stage of this design process, the leakage phenomenon has to be applied to the complete design. As it has been done for the simplified structure, only the horizontal magnetic plane of symmetry will be used. As well as in the previous section, small pieces of the *fictitious* dielectric have been included next to the ports of the structure. Having these considerations in mind, the final structure is detailed in Figure 3.20.

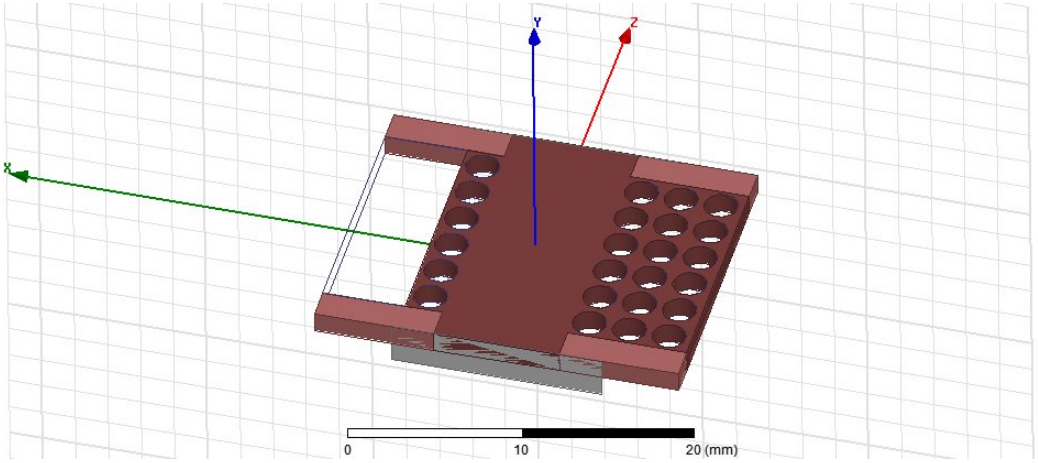

Figure 3.20: Complete design of the structure using the H symmetry plane of the LSM mode. ϵ_r=10. ϵ_{rholes}=5. a=2.54mm. b=7.62mm.

Performing a parametric analysis for the lateral distance d, the Scattering parameters and the value of α for different values of d have been obtained.

These results can be viewed in Figures 3.21 and 3.22. It can be appreciated that as the d is decreased, the radiation of the structure will be higher.

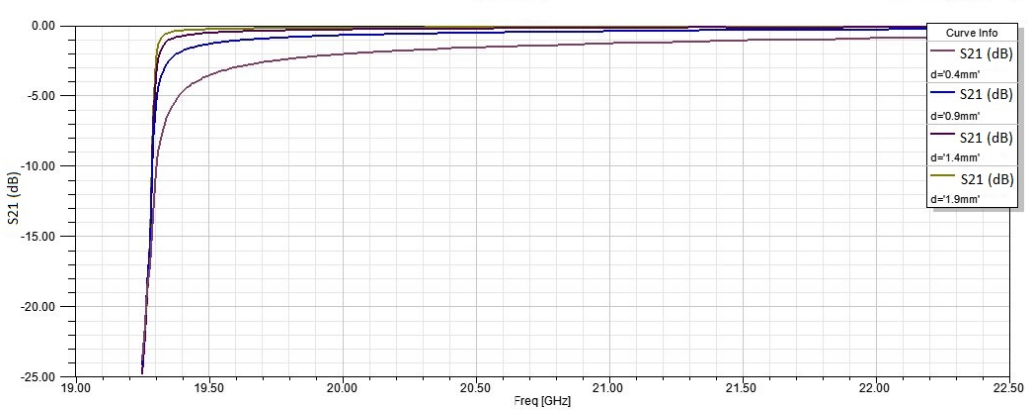

Figure 3.21: Representation of the Scattering parameters for the structure of Figure 3.20.

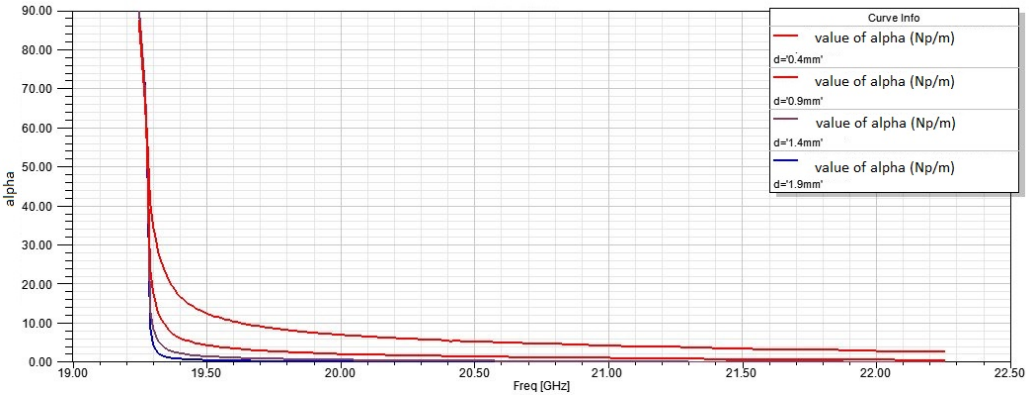

Figure 3.22: α in the structure of Figure 3.20.

It is interesting to notice that the value of d necessary to reach the leakage level obtained by the simplified model simulation has to be lower with the complete physical structure. The reason of this behaviour is that this model presents a softer transition between the central dielectric and the holes zone. As example, for a d value of 0.4 mm and 20 GHz of work frequency, in the complete model it is obtained a value of $\alpha = 7.2$ Np/m, meanwhile for the same scenario, in the simplified model it is obtained a value of $\alpha = 20.4$ Np/m.

Once the complete structure has been designed and simulated it is very interesting to obtain the radiation pattern of the leaky-wave antenna. The

structure, just because it is a waveguide, guide the energy introduced in the port 1 to the port 2. At the same time, part of this energy is radiated through the radiation face. The objective of the design of a leaky-wave antenna is to reduce the energy which arrives to the port 2 (and which will be dissipated by a matched load). At the same time, the objective is to increase the energy leaked to free-space in the form of radiation[1]. If there is not other losses in the structure, the percentage of leaked energy will define the $efficiency$ of the antenna. Once the structure has been designed and the leaky factor α has been obtained, the easiest way to increase the efficiency of the leaky-wave antenna is to increase the length of the waveguide, so more energy is radiated before it is delivered to port 2.

For the leaky antenna presented in this work, it has been fixed an efficiency goal of 90% which will be achieved through the variation of d (in order to increase α) and the length of the structure.

$$L = -\frac{1}{2\alpha}\ln(1-\eta) \tag{3.2}$$

$$1-\eta = \frac{|S_{21}|^2}{1-|S_{11}|^2} \tag{3.3}$$

The final value of d is 0.01 ($\alpha = 14.46Np/m$) mm with a length of 93.6 mm. The efficiency is easily calculated through the relations (3.2) and (3.2).

Under these conditions, the 3D directivity diagram is the one shown in Figure 3.23. However, it can be more interesting to study the radiation pattern in the XZ plane (see Fig. 3.20), the one controlled by our radiation parameters. This radiation pattern is shown in Figure 3.24, normalized to zero dB.

In order to verify these results, we can notice that the pointing angle of the antenna (θ_{max}) is around 36°-37° (knowing that 0° is the propagation direction). From the theoretical equations and with the relations (3.4) and (3.5), a θ_{max} of 38.2° is obtained, verifying the theory with a small error due to the simplified model used in the theoretical equations.

$$\cos\theta_{max} = \beta/k_{holes} \tag{3.4}$$

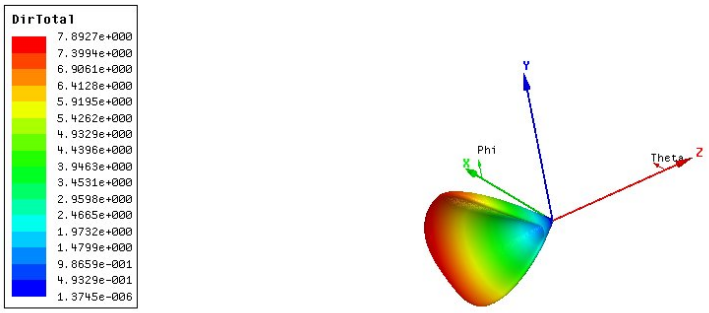

Figure 3.23: Representation of the directivity diagram in 3D (lineal).

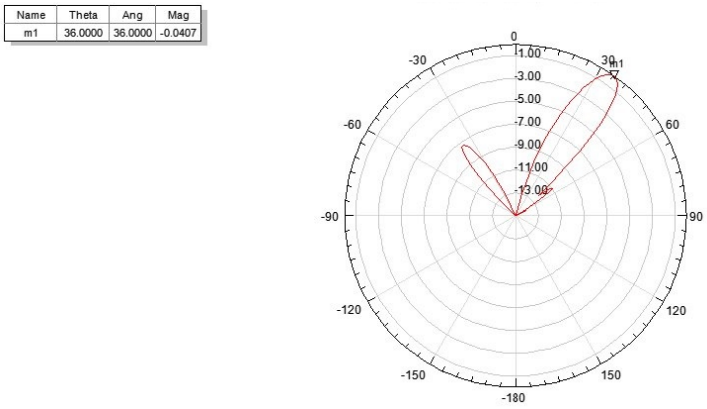

Figure 3.24: Representation of the normalized directivity diagram in the XZ plane (dB).

Frequency	20 GHz
Efficiency	93.3 %
Directivity Max.	7.892
Gain Max.	5.9195
Front to back ratio	32.69 dB

Table 3.1: Radiation parameters for the leaky-wave antenna presented

$$\theta_{max} = \arccos \frac{\beta c_0}{2\pi f} \tag{3.5}$$

The rest of the radiation parameters have been resumed in Table 3.1.

Observing Figure 3.24, a significant secondary lobe in the radiation pattern can be observed. This lobe is produced by the energy leaked through the air holes and can be significantly reduced decreasing the radio of these.

The last studies made to the antenna are the tests to demonstrate the frequency scanning phenomenon and how the parameters such as the radius of the holes and the distance d can be tuned to modify the radiation pattern.

In order to verify the frequency scanning behaviour presented in leaky antennas (due to the dispersive nature of the structure) we present in Figure 3.25 the radiation patterns obtained when the antenna is operated with different frequencies. It can be affirmed that if the work frequency is changed, consequently the β parameter varies, and through the relations described in 3.4 and 3.5 the pointing angle θ_{max} varies as well.

The possibility to tune our structure through physical parameters such as the holes radius and the distance d in order to adjust the radiation pattern can be very useful to improve the antenna electrical characteristics. In Chapter 2 it has been demonstrated that the variation of the $\epsilon_r holes$ causes a variation in the β factor, which is related with the pointing angle θ_{max}. In Figure 3.26 it is shown this relation between the radius of the holes and the maximum radiation angle.

The results displayed in Figure 3.26 show that it is possible to control the radiation angle or the β parameter through the tuning of the radius. In order to have a complete control of the radiation it will be necessary another

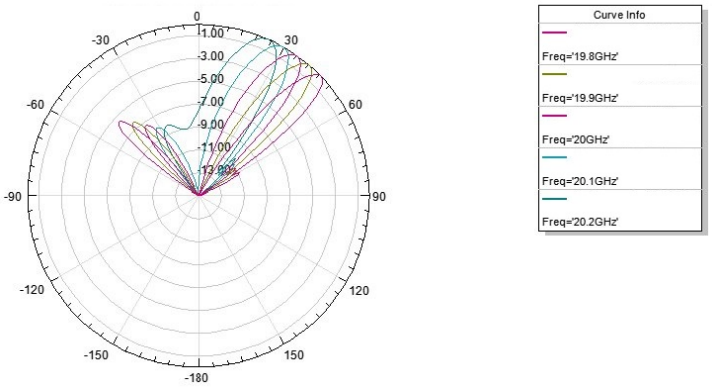

Figure 3.25: Representation of the normalized directivity diagram in the XZ plane (dB) for different frequencies.

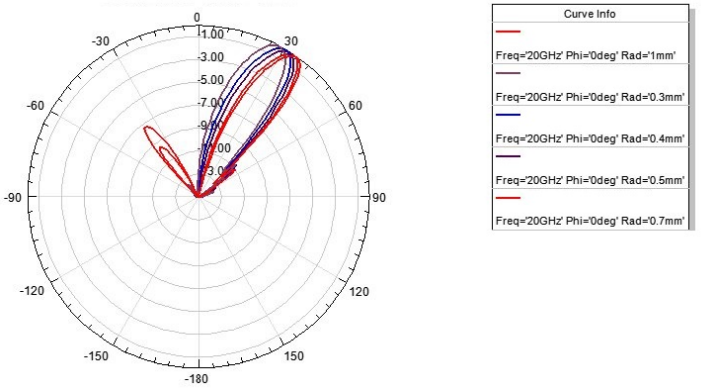

Figure 3.26: Representation of the normalized directivity diagram in the XZ plane (dB) for different values of the holes radius.

physical dimension to control the leakage parameter α. This is possible through the tuning of the distance d as it has been explained all along this chapter. To prove that this tuning does not affect to the parameter β we present the results in Figure 3.27. In this Figure for different values of d the pointing angle remains the same.

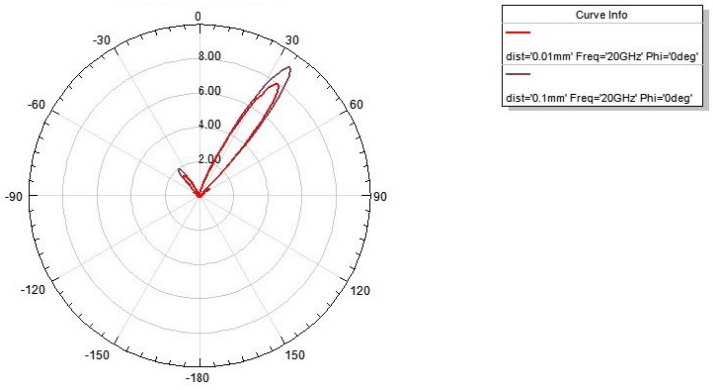

Figure 3.27: Representation of the normalized directivity diagram in the XZ plane (dB) for different values of d.

In summary it has been proven as possible a frequency scanning leaky-wave antenna in which the parameters α and β can be controlled separately.

Chapter 4

Proposal of the asymmetric SINRD (aSINRD): A novel SINRD-based waveguide

As result of the whole investigation and the several design processes carried out in this work, the idea of modificating the SINRD waveguide in order to change its performance has arisen. This Chapter is intended to propose a novel SINRD-based open waveguide and explain its theoretical foundations. In addition, this structure will be simulated and its response will be analysed.

The structure, conceived thanks to the symmetry planes of the NRD hybrid modes, has been called aSINRD (as abbreviation of asymmetric SINRD), due to its lack of symmetry in its horizontal plane.

4.1 Theoretical foundations of the aSINRD

The idea of the aSINRD arose while observing the planes of symmetry of the LSE and LSM hybrid modes and with the basis of the work developed in the creation of the image SINRD [24], [25]. In those works, the authors have analysed the symmetry planes of the LSM mode in a SINRD structure and have taken advantage of the electric field symmetry plane placed in the vertical plane of the structure. By using a perfect electric conductor (PEC) in

this plane, the size of the SINRD has been halved. Consequently, the number of modes in the resulting image SINRD (iSINRD) guide is equally reduced since all even modes including the LSE modes are suppressed. Details of the explanation of the iSINRD idea and its hybrid mode are shown in Fig. 4.1.

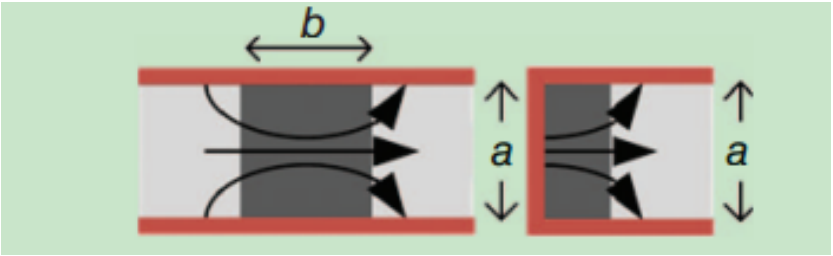

Figure 4.1: Transformation from SINRD to iSINRD structures.

The fundamentals of the aSINRD guide are similar, however, in this case it has been intended to take advantage of the magnetic field symmetry plane placed in the horizontal plane of the structure presented in both LSM and LSE modes. Following the same concepts as with the iSINRD structure, by using a perfect magnetic conductor (PMC) in this plane, the size of the SINRD could be halved. However, the impossibility to find this kind of PMC materials in nature and the complexity of the artificial PMC techniques makes harder the designing and building process of this structure.

Is for this reason that the effect of placing a PMC in the symmetry plane has been achieved by creating a magnetic wall effect by placing a high dielectric permittivity gap between the waveguide material and the air. Through this technique, used for instance in a dielectric rod waveguide [1], it is theoretically possible to create a magnetic wall effect which could substitute the magnetic field plane symmetry presented in both LSM and LSE hybrid modes.

In summary, the aSINRD is an open waveguide where the thickness of the dielectric is half of the SINRD vertical size. The details of the aSINRD structure and how the LSE mode remains is shown in Figure 4.2.

It is important to remind that the working principle of the SINRD waveguide is to mantain $\beta < k_{holes}$ in order to keep the confinement condition caused by the parallel plates, that keeps the mode below cutoff in the region filled with holes. In the aSINRD structure, due to its open side it is necessary to maintain $\beta > k_0$ in order to maintain the wave confined in the dielectric in the open side. Therefore, the necessary condition to work with the aSINRD

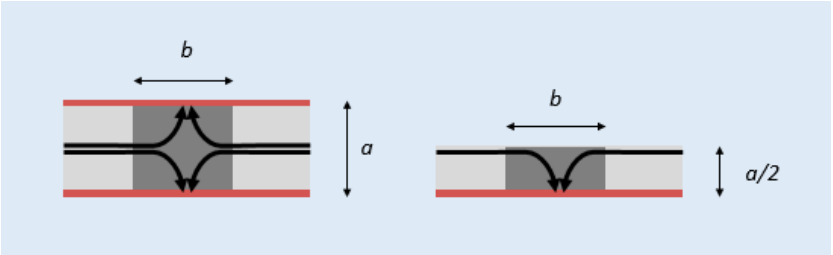

Figure 4.2: Transformation from SINRD to aSINRD structures and electric field lines for the LSE mode.

is $k_0 < \beta < k_{holes}$.

4.2 aSINRD performance

Once the idea of the aSINRD guide has been presented, several simulations of this structure have been carried out in order to demonstrate its performance. The design parameters have been chosen to be similar to the ones selected in Chapter 3, however, some of these have been changed to fit better with the aSINRD requirements.

The analysed structure has the following design parameters:

- $a = 2.7mm$ (see Fig. 4.2).
- $b = 2.54mm$ (see Fig. 4.2).
- Used material dielectric: Taconic CER-10. $\epsilon_r = 10$. $tan\delta = 0.0035$.
- Working frequency=20 GHz.
- Radius of the holes=1mm.

The effective permittivity of the holes zone has been designed for a value of 7.

The design starts with the frequency response analysis of the structure through the theoretical equations in order to differentiate the working frequency band. As it has been explained, the working frequency band has to fullfil the next relation:

$$k_0 < \beta < k_{holes} \tag{4.1}$$

which, with a simple operation becomes:

$$1 < \beta/k_0 < \sqrt{\epsilon_{r_{holes}}} \tag{4.2}$$

therefore, knowing that $\sqrt{\epsilon_{rholes}} = 2.6458$, the representation of β/k_0 for each frequency will show the working frequency band of the structure. The corresponding graphic is shown in Fig. 4.3

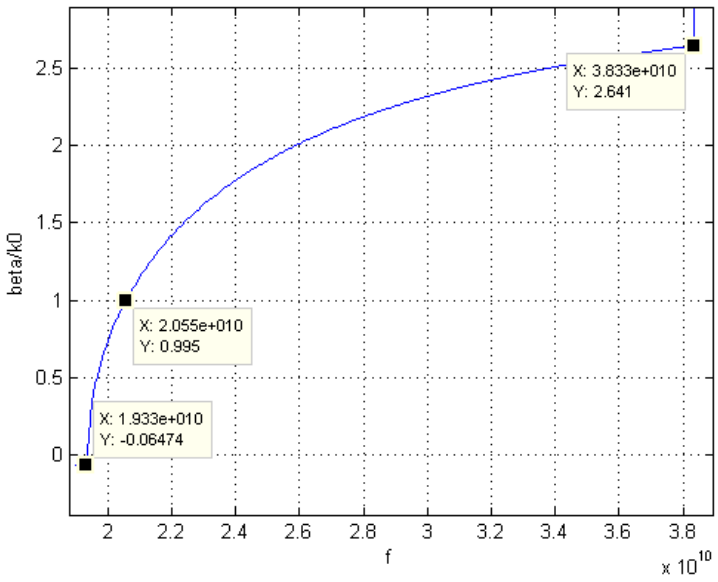

Figure 4.3: β/k_0 as a function of the working frequency.

Three regions can be differentiate in Fig. 4.3. In the first place it can be affirmed that the cutoff frequency of the LSE mode is at 19.33 GHz, since $\beta = 0$ at this frequency. From this cutoff frequency to 20.55 GHz the energy of the mode is propagative inside the structure but leaky in the open face (region where $\beta < k_0$). From 20.55 GHz to 38.33 GHz the energy is propagative in the structure and not leaky in the open face, in other words, this is the desirable frequency band to operate the structure as a guiding device.

Once the frequency analysis has been carried out, the structure has been simulated in HFSS in order to validate the theoretical results and to obtain the Scattering parameters of the structure.

The representation of the module of the electric field inside the structure is shown in Fig. 4.4 and Fig. 4.5. It can be affirmed that the energy remains guided inside the waveguide.

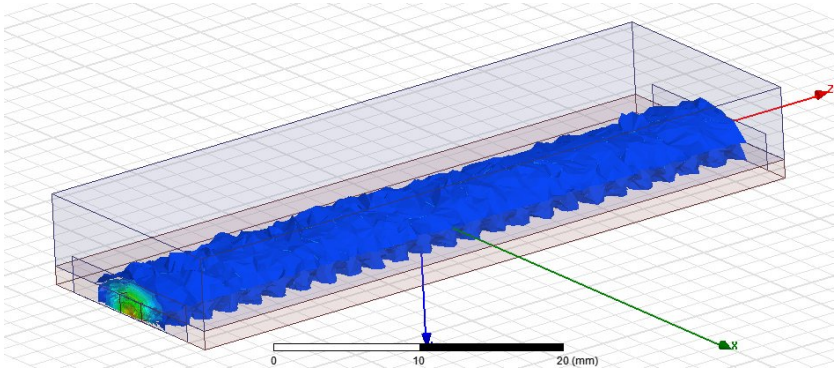

Figure 4.4: Representation of the electric field module in the aSINRD waveguide (region above the structure).

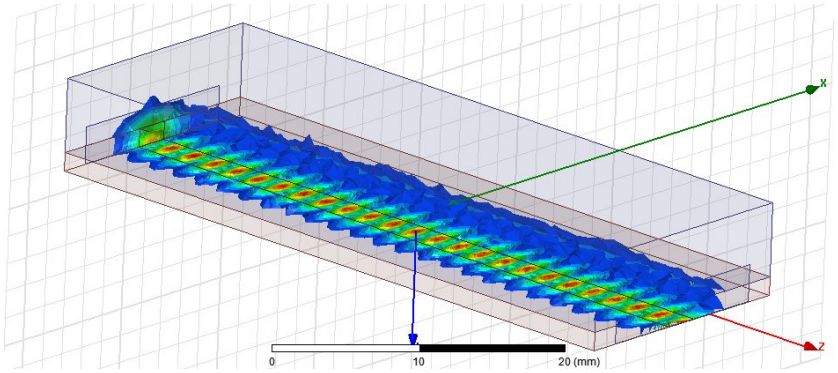

Figure 4.5: Representation of the electric field module in the aSINRD waveguide (region below the structure).

The Scattering parameters are shown in Figure 4.6. In the chart it can be observed the three regions presented in Figure 4.3. In this case, the cutoff frequency does not appear so clear due to the open character of the waveguide, which turns into radiation the energy that is reflected in the SINRD closed waveguide. From this cutoff frequency of 19.33 GHz to 20.55 GHz the energy starts to be guided but it is radiated in the open space as it

has been explained. From 20.55 GHz and above the energy remains guided and the losses are minimal. It can also be observed that the matching of the structure is very good in all considered frequency range.

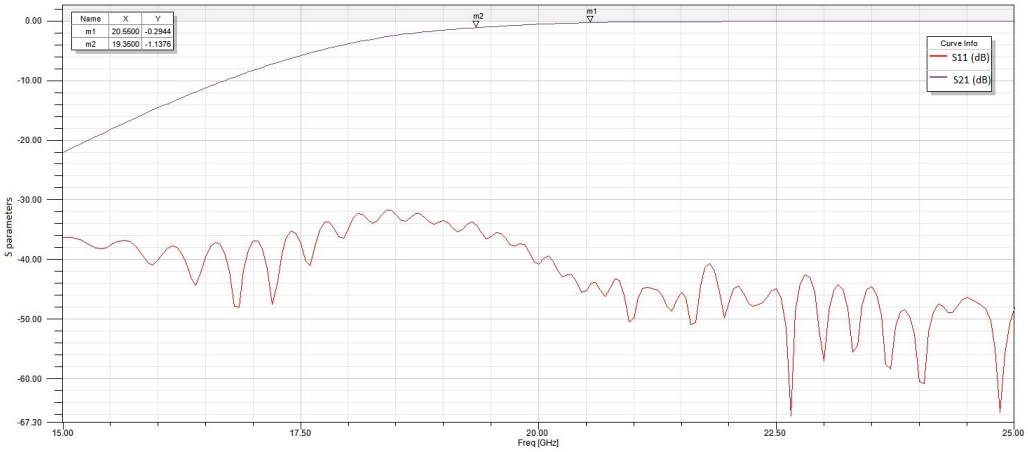

Figure 4.6: Representation of the Scattering parameters for the aSINRD waveguide.

4.3 Proposal of an aSINRD based leaky-wave antenna

The aSINRD waveguide has been proposed and its response has been analysed and verified. As it has been explained, the aSINRD is an open structure, therefore, the idea of making it radiative through this open face comes natural. In this section it is aimed to propose the concept of a novel leaky-wave antenna based on the aSINRD structure presented in the previous section.

The aSINRD open face bases its operation on creating a high difference of permittivity between the guide and the air, creating in this way a magnetic wall effect. The idea is similar to the early dielectric rod based waveguides [24],[25], and, the idea of creating a leaky-wave antenna from this waveguide has been studied in several works [1]. In those works it is investigated the possibility of making the structure to radiate by introducing discontinuities over one face of the rectangular dielectric rod. These discontinuities can be made with a grating of grooves and with a grating of metal strips as it is shown in Fig. 4.7. However the metal strips option has been demonstrated to

be a better choice in terms of bandwidth and versatility of radiation beams. Therefore, and also because of its facility in terms of construction, the structure with the metal strips has been chosen to be investigated over the aSINRD guide.

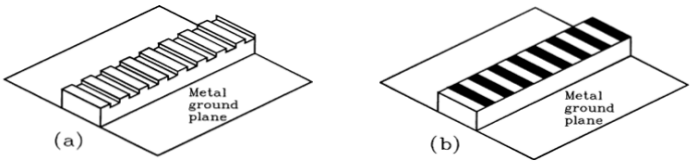

Figure 4.7: Dielectric image guide with (a) a grating of grooves and (b) a grating of metal strips.

Having these concepts in mind, periodic metal strips has been introduced over the open face of the aSINRD guide. When a periodic leaky-wave structure is designed it is important to know that the dominant mode is slow-wave relative to free-space velocity. Therefore the dominant mode itself does not radiate and it needs the periodic modulation to produce the radiation.

In order to study and design a leaky-wave periodic structure it is necessary to introduce the concept or space harmonics. When the periodic array of strips is added, the periodicity introduces an infinity of space harmonics, each characterized by phase constant β_n related to each other by

$$\beta_n p = \beta_0 p + 2\pi n \tag{4.3}$$

where p is the period and β_0 is the fundamental space harmonic. β_n can take a huge variety of values, leading to forward or backward waves, and fast or slow waves. Since the structure is open, a space harmonic that is fast will radiate. In summary, as it is needed a single radiation beam, it will be designed a structure where only one space harmonic will be fast, and will radiate. The easiest way is to choose the harmonic β_{-1} to be the operational mode. In consequence, the physical parameter d will be selected to ensure this condition.

Having these design parameters in mind, it has been designed the structure of a leaky-wave aSINRD as shown in Fig. 4.8. The radiation pattern obtained is shown in Figure 4.9 in 3D and in Figure 4.10 depending of the value of the parameter d, which indicates the periodicity of the grating.

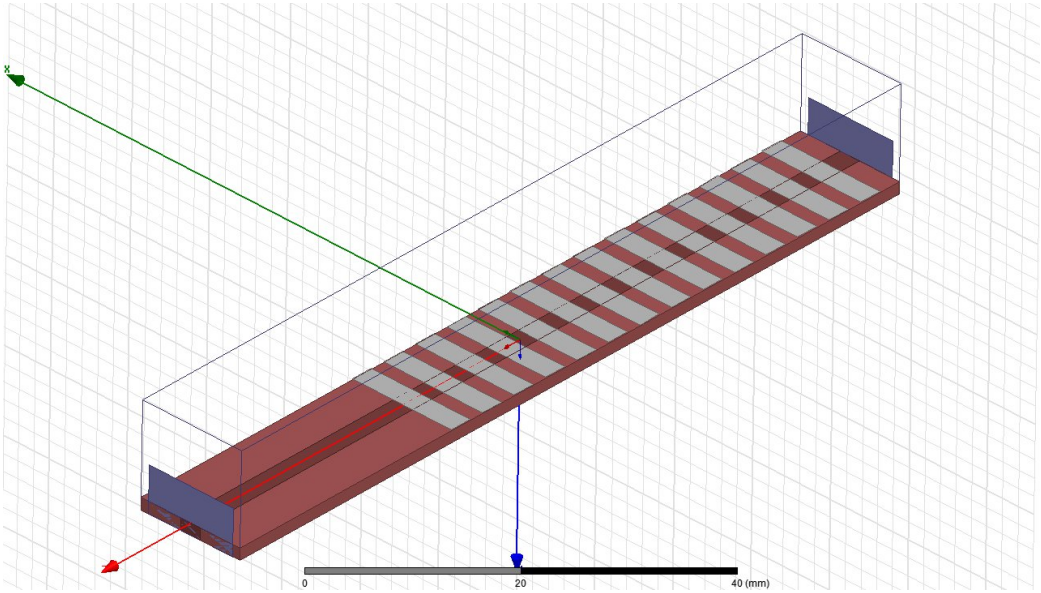

Figure 4.8: Structure of the leaky-wave aSINRD.

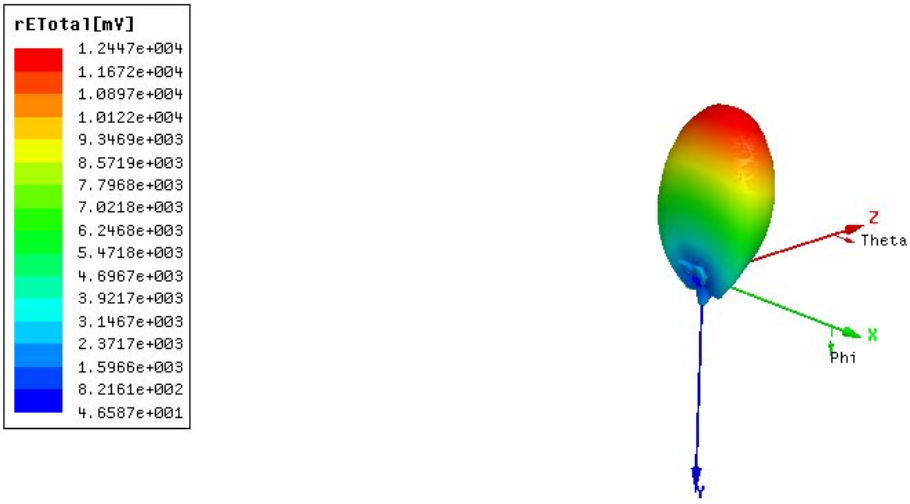

Figure 4.9: Radiation Pattern of the leaky-wave aSINRD in 3D

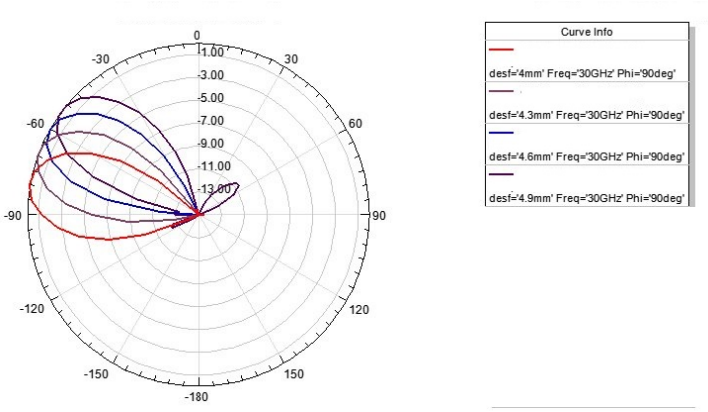

Figure 4.10: Radiation Pattern of the leaky-wave aSINRD when the period d is changed

Chapter 5

Construction of an aSINRD waveguide prototype

In Chapter 4, the aSINRD was introduced. This novel waveguide was presented as a modification of the SINRD waveguide using one of the symmetry planes of the LSE hybrid mode (see Fig. 4.2). In order to support the theoretical work realised in Chapter 4, the construction of an aSINRD prototype was undertaken. This chapter has the aim of detailing the whole construction work as well as verifying the results obtained in Chapter 4.

5.1 The feeding circuit

In Section 2.4 of Chapter 2 the problematic of feeding the hybrid modes in a SINRD structure was introduced. The field distribution of these modes makes harder to feed these modes with traditional transmission lines. However, with the proposal of the aSINRD waveguide, it has been noticed that the field distribution of the LSE hybrid mode of the aSINRD (see Fig. 5.1) was similar to the field distribution of a microstrip line (see Fig. 5.2). As result of this field destribution *matching*, a microstrip into aSINRD transition has been proposed.

The proposed transition is shown in Fig. 5.3. The transition consist of a first section of microstrip line in which the conductor is tapered until

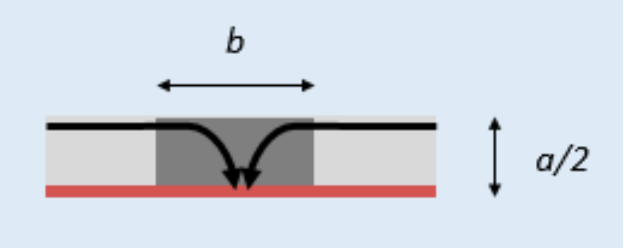

Figure 5.1: Field lines of the LSE hybrid mode in the aSINRD.

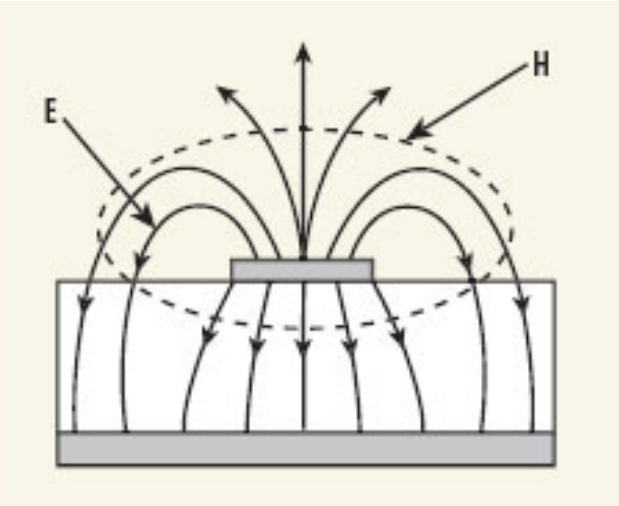

Figure 5.2: Microstrip field lines.

getting a pointly ending placed inside the aSINRD. The ground plate of the microstrip is shared with the aSINRD plate.

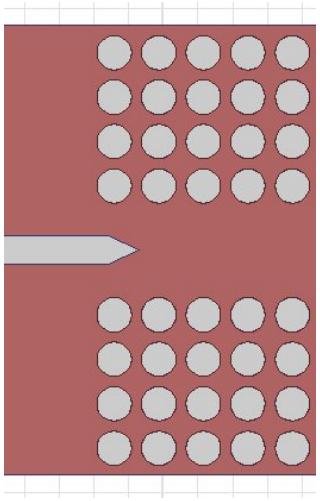

Figure 5.3: Microstrip into aSINRD transition layout.

The result is a good matching between the transmission line and the waveguide that can be improved by optimising the length of the tapering. In the design realised, the length of the tapering has been optimised through a quasi-newton algorithm provided by the HFSS software. Once the optimisation has been realised, the distribution of the electric field is shown in Fig. 5.4. Also the Scattering parameters are shown in Fig. 5.5. It can be noticed that the two transitions of the structure introduce about 1 dB of losses. This lost power is radiated to the exterior due to the open nature of the aSINRD.

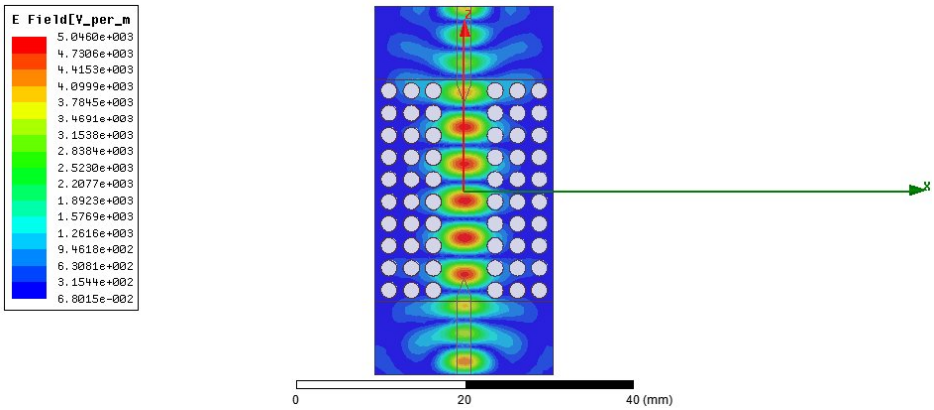

Figure 5.4: Electric field distribution of the microstrip to aSINRD transition.

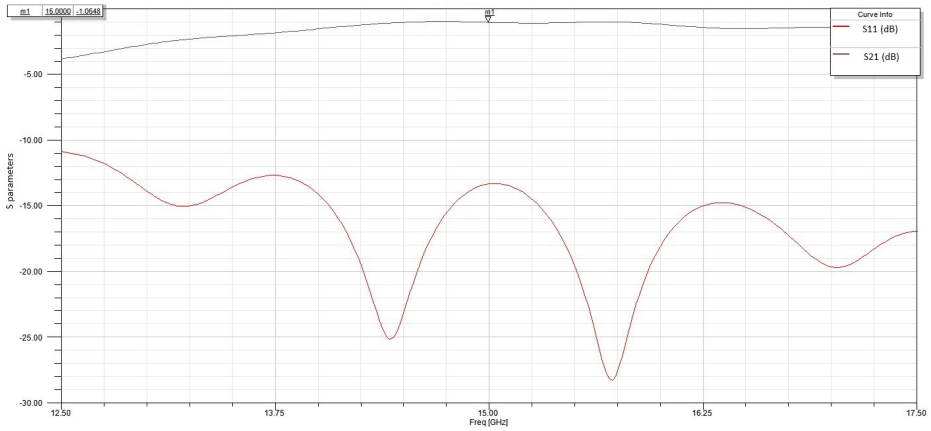

Figure 5.5: S parameters of the microstrip to aSINRD transition.

5.2 Design of the whole prototype

Once the feeding circuit has been chosen, the whole prototype to build has been designed. As it has been explained in Chapter 3, the design parameters have to fit with the laboratory facilities. Following the laboratory restrictions detailed in Chapter 3, it has been designed an aSINRD waveguide with the following design parameters

- The cutoff frequency of the waveguide is designed to be 11 GHz. The operating band will be 12.5-17.5 GHz.
- The material used for the substrate is the Taconic CER-10 which has a dielectric constant of 10 and a thickness of 1.27 mm. It will be used two layers in order to increase the thickness.
- The material used to glue the two layers will the Taconic Tacbond. A microwave bonding film [10]. It presents a dielectric constant of 2.35 and 38 μm of thickness.
- The diameter of the holes is fixed to 2 mm getting an effective permittivity in the holes zone of 7.
- $a = 5.44mm$
- $b = 5.08mm$
- $L = 28.227mm$

With this scenario, the structure of Fig 5.6 has been designed. The Scattering parameters for the operating band are shown in Fig 5.7. Observing the Scattering parameters can be noticed substantial losses in the S_{21} parameter. As it has been demonstrated in Section 5.1, almost 1 dB of power lost is due to the microstrip to aSINRD transition. The rest of the losses are due to the Taconic CER-10, which presents a $tan\delta$ of 0.0035. Also there are some quasi-negligible losses due to the Taconic Tacbond layer.

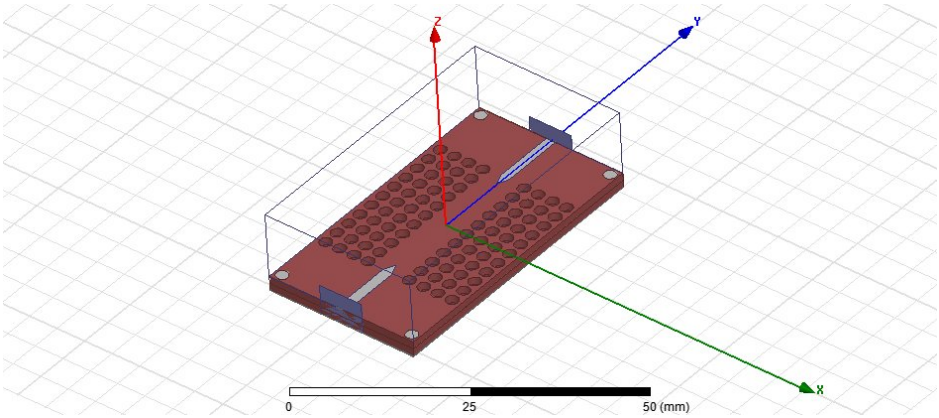

Figure 5.6: Layout of the aSINRD prototype.

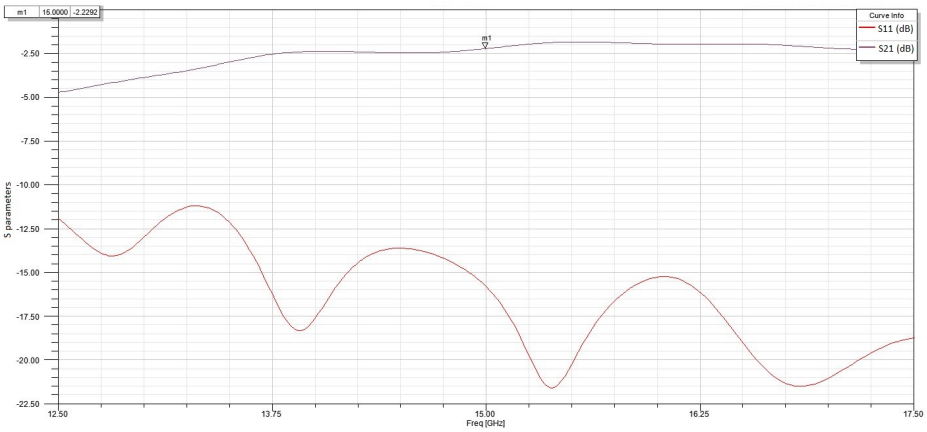

Figure 5.7: S parameters of the aSINRD prototype designed.

5.3 The construction process of the prototype

The construction process has been completely done at the Microwaves Laboratory of the University of Pavia. This laboratory provides the minimum resources for building a circuit prototype at high frequency. The resources are the following:

- The simulation sofware HFSS to evaluate the response of the whole circuit.
- The electronic design software Advanced Design System (ADS) to create a layer based design.
- The LPKF Protomat E-33 and its controlling software. A milling/-drilling machine which will serve to create the circuit from the layer based design.
- Several measurements devices such as Network analysers, Oscilloscopes, etc.

The construction flow followed in the building of the aSINRD prototype is shown in Fig. 5.8.

The simulation of the whole circuit

The design process has been explained in Section 5.2, and the results presented in Fig. 5.7. This design and results will be the starting point for the construction process. It is crucial to design a prototype as accurate as possible in order to control the most part of the construction parameters. In the design realised has been included elements such as the Tacbond and the two layers structure in order to know how they affect to the prototype.

As it has been said, the design has been realised with the HFSS simulation software. The laboratory provides dedicated computers to this software and to the simulation task.

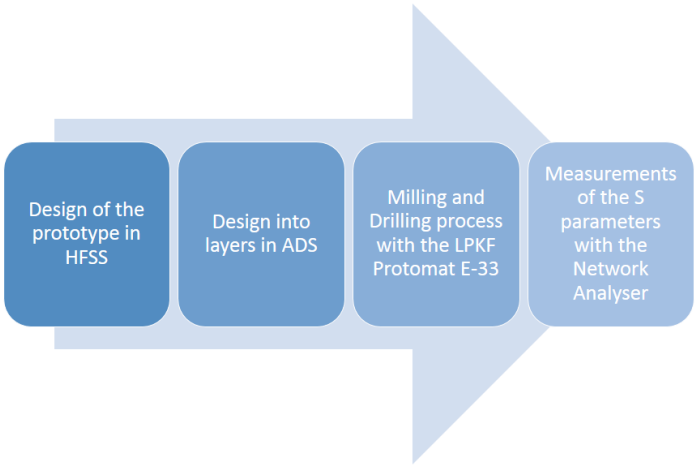

Figure 5.8: Construction flow followed in the building of the aSINRD prototype.

The layers design

In order to indicate the milling/drilling machine how the prototype must be built, it is mandatory to give the design to the machine in a proper format. This milling/drilling machine works with the .ads format and in the provided file the design must be divided in layers. To realise this work the software Advanced Design System(ADS) has been used. This software is capable of reading a .gds file imported from HFSS, modifying the layers of the circuit and exporting the whole design to a .ads file. A screenshot of this software is shown in Fig. 5.9.

The milling/drilling process

Once the design has been converted into the proper .ads format and it has been divided into layers, the milling/drilling machine can start to elaborate the circuit. The milling/drilling machine used is shown in Fig. 5.10.

This machine is able to elaborate a microwave circuit from a piece of dielectric with a metallic shield (see Fig. 5.11). These pieces of shielded

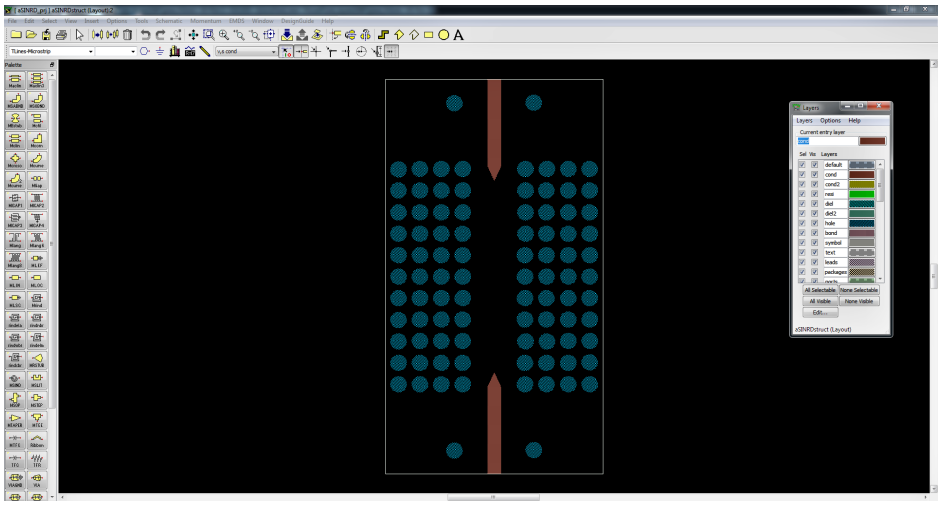

Figure 5.9: Screenshot of the ADS software designing the aSINRD prototype.

Figure 5.10: Photography of the LPKF protomat e-33 machine. Provided by LPKF USA.

dielectric material are directly sold by the manufacturer, in this case Taconic. From these pieces, the machine will drill the holes in first place, and it will mill the metallic layer to create the required pattern (in this case, two microstrip feeding lines).

Figure 5.11: Photography of a piece of shielded dielectric material.

The pieces resulting of the milling/drilling process are shown in Fig. 5.12. As it has been explained in Chapter 4 the construction has been made in two layers because of the materials available. In the next step the layers will be glued.

Previously to the measurements, the circuit must be prepared for being connected with the measurements devices. This step could be skipped depending on the circuit projected. In this case, the circuit has to be worked in order to adapt it to the network analyser. This preparation consist basically in two steps, the junction of the two layers and the incorporation of the SMA connectors.

The junction of the two layer has been realised by a material called Tacbond as Section 5.2 details. The glue process consist of introducing a layer of Tacbond between the two aligned layers of the circuit and heating the whole piece 1 hour at 200° in an oven.

The employed connectors are the End Launch connectors by Southwest Microwave. This removable connectors have the advantage of not being in-

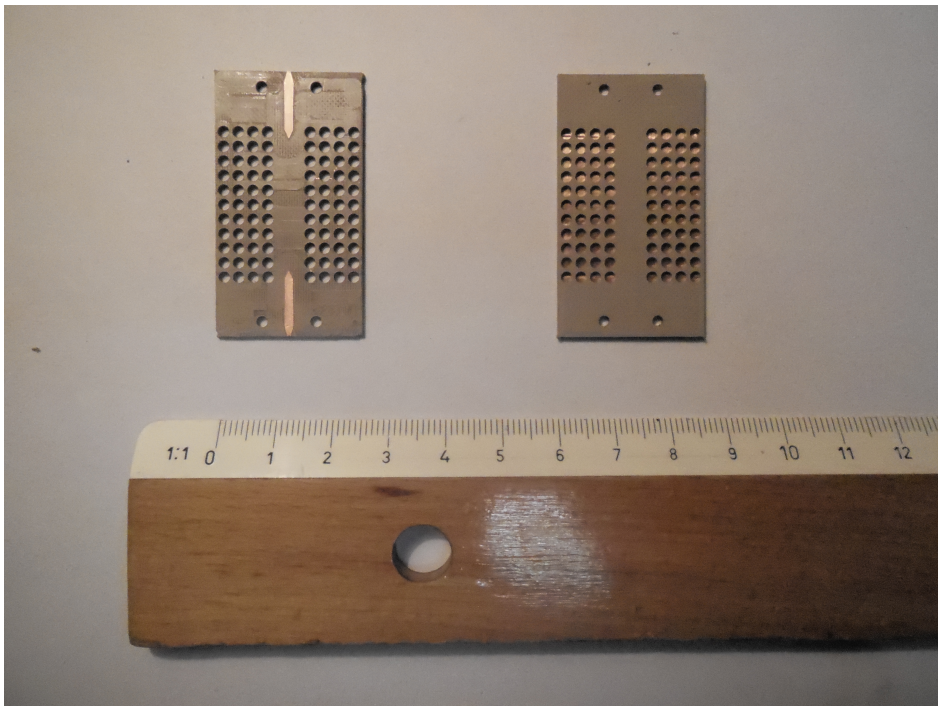

Figure 5.12: Photograph of the resulting pieces from the milling/drilling process.

corporated to the circuit by a welding process. The connectors have a screw system which allows a removable incorporation. The connectors are shown in Fig. 5.13.

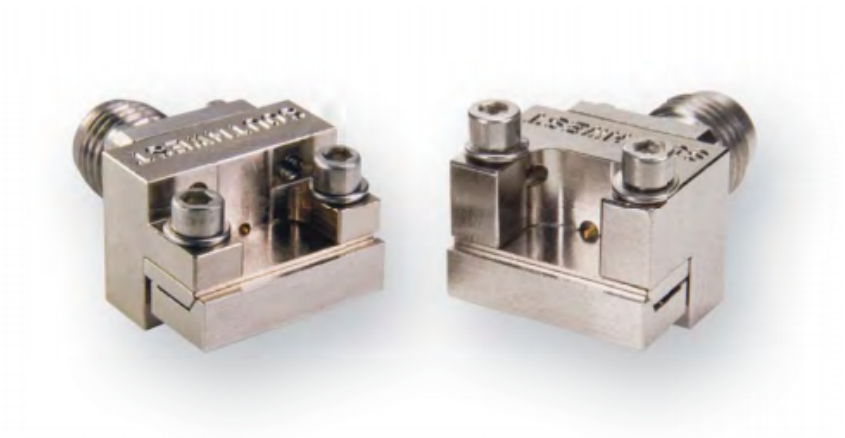

Figure 5.13: Photography of the connectors used in the prototype. Provided by Southwest Microwave.

The prototype after being prepared for the measurements is shown in Fig. 5.14

The measurements

The measurement process for this waveguide consist of extracting the Scattering parameters for the frequency band desired. This process has been undertaken by a network analyser, in this case the Anritsu 37347C. The measurement disposition is shown in Fig. 5.15.

The results obtained, confronted with the simulated ones are shown in Fig. 5.16. A deviation of about 2 dB between the measurements and the simulations can be appreciated which it is related with the artisan manufacturing process. However, the guiding phenomenon of the aSINRD is proven.

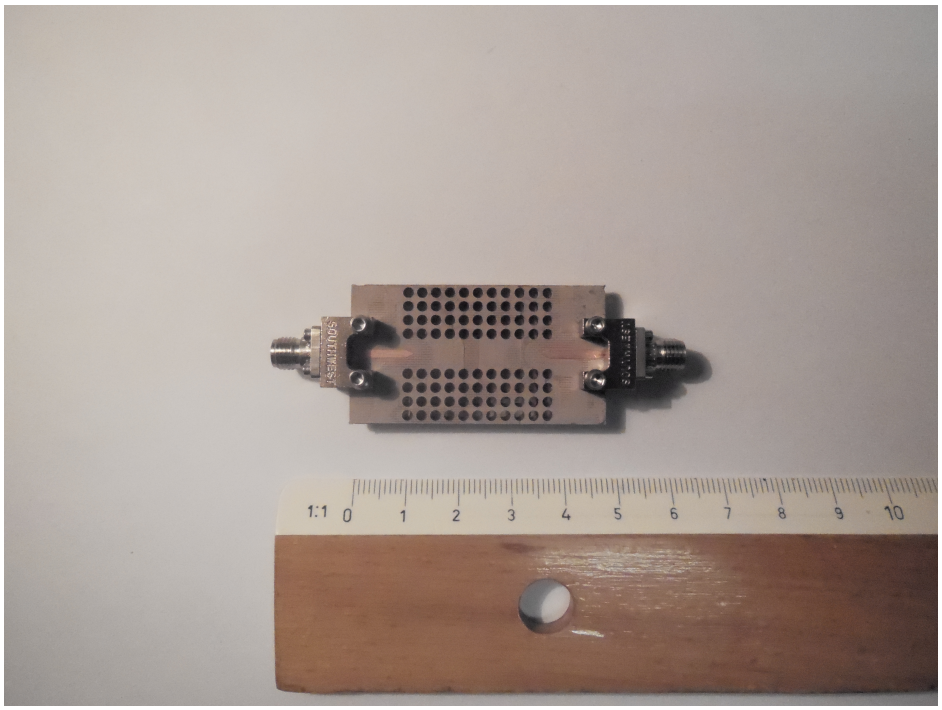

Figure 5.14: Photography of the prototype realised ready for the measurement process.

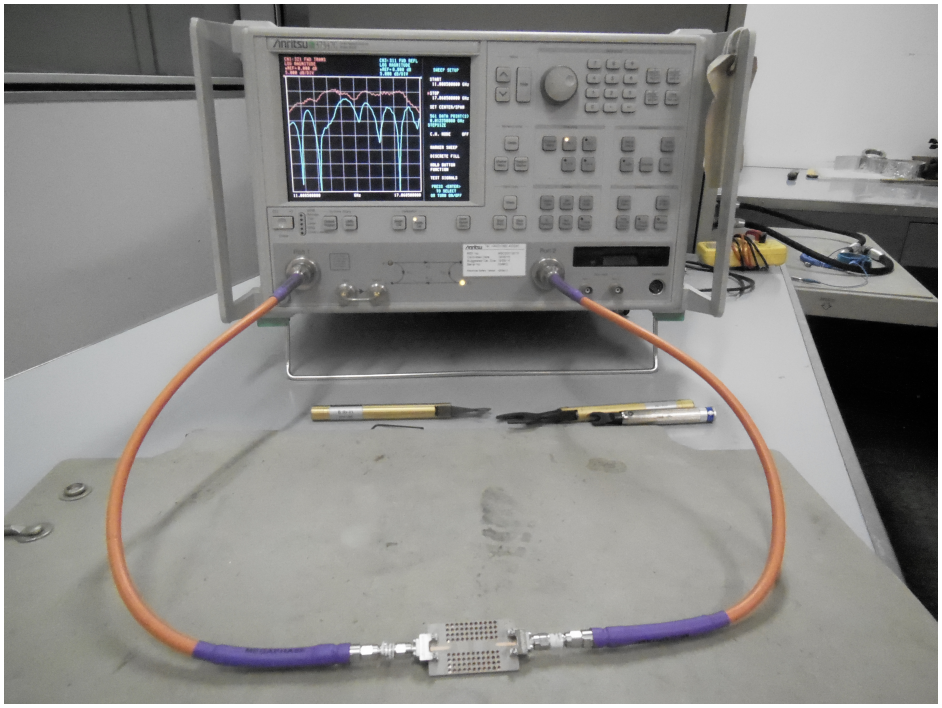

Figure 5.15: Photography of the measurement disposition with both the network analyser and the circuit.

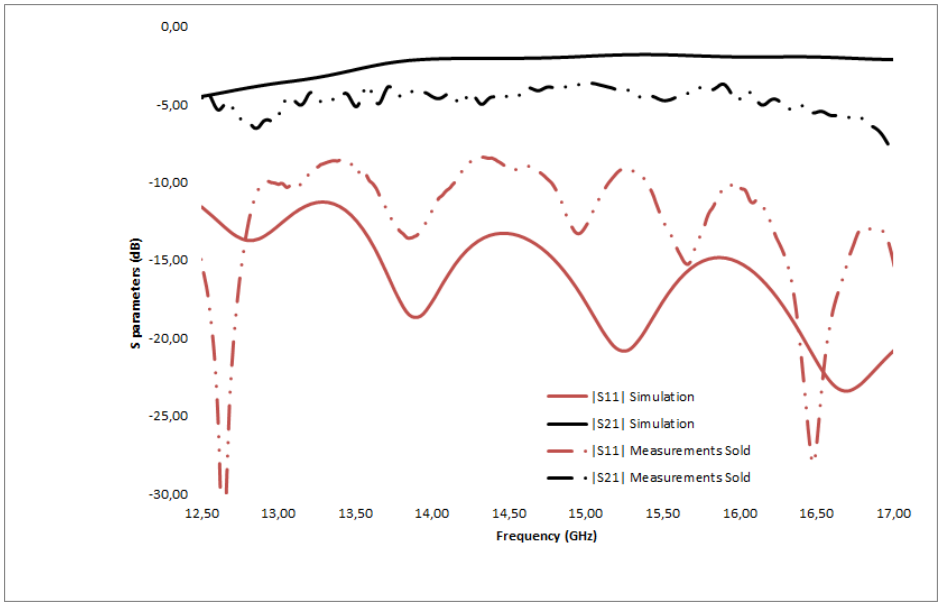

Figure 5.16: Results obtained for the measurement process confronted with the simulated results.

Conclusions and Future Work

Due to the different topics studied in this work, the conclusions obtained are several. In one hand, the possibility of implementing a leaky-wave antenna based on SINRD technology has been proven. Starting from an early leaky-wave antenna designed in the 80's by Sanchez and Oliner[2], it has been designed a proper leaky-wave antenna with a good performance and configurable through the design parameters.

The NRD and its planar adaptation, the SINRD, are an optimal choice in the designing of microwave devices at high frequencies. The difficulties associated to the excitation of hybrid modes are compensated with its good performance and the possibilities the structure offers to make it leaky.

On the other hand, a novel waveguide based on the NRD guide has been proposed, the so-called aSINRD. Its performance has been studied and a proposal of leaky-wave antenna based on this aSINRD has been introduced. In addition, the guiding phenomenon of the aSINRD has been proven with the manufacturing of a prototype with real components. The results demonstrate the possibility of using this waveguide in future practical designs.

A more accurate study of the response in the holes zone of the SINRD and a deep research about the possibilities the aSINRD offers, are proposed as future lines of this work. Also, a tapered design of the leaky-wave SINRD based on the holes geometry will improve the radiation performance obtained. The possibilities that these technologies offer are too huge for being attended in this work, however the starting point for some of them has been described.

Bibliography

[1] John Volakis. *Antenna Engineering Handbook*, chapter 11: Leaky-Wave Antennas.

[2] Alberto Sanchez and Arthur A. Oliner. A new leaky waveguide for millimeter waves using nonradiative dielectric(nrd) waveguide - part i: Accurate theory. *IEEE Transactions on Microwave Theory and Techniques, VOL. MTT-35, NO. 8*, August 1987.

[3] Abdallah Bacha and Ke Wu. Toward an optimum design of nrd-guide and microstrip-line transition for hybrid-integration technology. *IEEE Transactions on Microwave Theory and Techniques, VOL. 46, NO. 11, pp. 1796-1800*, Nov 1998.

[4] Feng Xu and K. Wu. Substrate integrated nonradiative dielectric waveguide structures directly fabricated on printed circuit boards and metallized dielectric layers. *IEEE Transactions on Microwave Theory and Techniques, VOL. 59, NO. 12, pp. 3076-3086*, Dec 2011.

[5] W. W. Hansen. Radiating electromagnetic waveguide: U.s. pat. 2,402,622. 1940.

[6] Takanori Okoshi and Tanroku Miyoshi. The planar circuit — an approach to microwave integrated circuitry. *IEEE Transactions on Microwave Theory and Techniques, VOL. MTT-20, NO. 4*, April 1972.

[7] Yuanxin Li, Quan Xue, Edward Kai-Ning Yung, and Yunliang Long. Dual-beam steering microstrip leaky wave antenna with fixed operating frequency. *IEEE Transactions on Antennas and Propagation, VOL. 56, NO. 1*, January 2008.

[8] David R. Jackson Juhua Liu and Yunliang Long. Substrate integrated waveguide (siw) leaky-wave antenna with transverse slots. *IEEE Transactions on Antennas and Propagation, VOL. 60, NO. 1*, January 2012.

[9] T. Yoneyama and S. Nishida. Nonradiative dielectric waveguide for millimeter-wave integrated circuits. *IEEE Transactions Microwave Theory Technology, VOL. MTT-29, pp. 1188-1192*, Nov 1981.

[10] Taconic. Ht 1.5 rf and microwave bonding film [on line]. *http://www.taconic-add.com/en–products–ht15–1.php*, 09/03/2015 [consulted 10 Mar 2015].

[11] T. Yoneyama and S. Nishida. Nonradiative dielectric waveguide circuit components. *presented at the Int. Conf. Infrared and Millimeter Waves, Miami, FL*, Dec 1981.

[12] Arthur A. Oliner Han Qing and Alberto Sanchez. A new leaky waveguide for millimeter waves using nonradiative dielectric(nrd) waveguide - part ii: Comparison with experiments. *IEEE Transactions on Microwave Theory and Techniques, VOL. MTT-35, NO. 8*, August 1987.

[13] F. J. Tischer. A waveguide structure with low losses. *Arch. Elec. Uebertragung, vol. 7, pp. 592-596*, December 1953.

[14] L. A. Weinstein. The theory of diffraction and the factorization method (translated from russian). boulder, co:golem press, pp. 29-50. 1969.

[15] H. M. Altschuler and L. O. Goldstone. On network representations of certain obstacles in waveguide regions. *IRE Trans. Microwave Theory Tech., vol. MTT-7, pp. 213-221*, April 1959.

[16] Miroslav Balda. cxroot - complex root of complex function [on line]. *http://www.mathworks.com/matlabcentral/fileexchange/22661-cxroot-complex-root-of-complex-function/content/cxroot.m*, 12 Jan 2009 [consulted 21 Nov 2014].

[17] Y. Cassivi and K. Wu. Substrate integrated non-radiative dielectric waveguide. *IEEE Microw. Wireless Compon. Lett., vol. 14, no. 3, pp. 89-91*, Mar. 2004.

[18] Y. Cassivi and K. Wu. Substrate integrated circuits applied to the nonradiative dielectric guide. *Proc. Inst. Elec. Eng.- Microw., Antennas, Propag., vol. 152, no. 6, pp. 424-433*, Dec. 2004.

[19] Y. Cassivi and K. Wu. Substrate integrated nrd (sinrd) guide on high dielectric constant substrate for millimeter wave circuits and systems. *IEEE MTT-S Digest, pp. 1639-1642*, 2004.

[20] Priyanka Mondal and Ke Wu. A leaky-wave antenna in substrate integrated non-radiative dielectric (sinrd) waveguide with controllable scanning rate. *IEEE Transactions on Antennas and Propagation, VOL. 61, NO. 4*, April 2013.

[21] José Capmany, F. Javier Fraile Peláez, and Javier Martí. *Fundamentos de Comunicaciones Ópticas*. Síntesis, 1998. ISBN 8477385998, 9788477385998.

[22] Jinbang Tang and Ke Wu. Integrated microstrip to nrd-guide transition using a spurious mode suppressing technique. *IEEE MTT-S Digest, pp. 1805-1808*, 2000.

[23] Wolfgang Menzel Ulf Schmid. Planar antenna arrays using a feed network with nonradiative dielectric(nrd) waveguide. *Proc. 'EuCAP 2006', Nice, France 6–10 November 2006 (ESA SP-626, October 2006)*, 2006.

[24] Jawad Attari. The image substrate integrated non-radiative dielectric waveguide for low-loss millimeter-wave applications. *IET Microwaves, Antennas and Propagation*, 2013.

[25] Tarek Djerafi Jawad Attari and Ke Wu. Fast and accurate simulation of novel millimeter-wave circuits based on commercial software package. *IEEE Microwave Magazine, 1527-3342*, 2013.

Appendix A

Matlab Codes:
nrd_leaky_function.m

```
function [out]=nrd_leaky_function(beta)

global d;
global k0;
global a;
global b;
global EpsR;
global f;
global lambda0;
n=1;

w=2*pi*f;
Mu0=pi*4e-7;
Eps0=8.8541878176e-12;
c0=1/sqrt(Mu0*Eps0);
lambda0=c0/f;
Eps=Eps0*EpsR;

k0=(2*pi)/lambda0;
k=k0*sqrt(EpsR);

betaMax=k0*sqrt(EpsR);

kx=n*pi/a;

ky=sqrt(k^2-kx^2-beta.^2);
ky=abs(real(ky))-1i*abs(imag(ky));
```

```
ky_air=sqrt(k0^2-kx^2-beta.^2);
ky_air=abs(real(ky_air))-1i*abs(imag(ky_air));

%Impedancias de los modos (dielectrico)
Ze_TMz=(EpsR*k0^2-(beta).^2)./(ky*w*Eps);
Ye_TMz=1./Ze_TMz;

Ye_TEz=(EpsR*k0^2-(beta).^2)./(ky*w*Mu0);
Ze_TEz=1./Ye_TEz;

%Impedancias de los modos (aire)
Z0_TMz=(k0^2-(beta).^2)./(ky_air*w*Eps0);
Y0_TMz=1./Z0_TMz;

Y0_TEz=(k0^2-(beta).^2)./(ky_air*w*Mu0);
Z0_TEz=1./Y0_TEz;

%Factor de acoplo
N=((k0^2)*(EpsR-1)*(beta)*(pi/a))./((k0^2-(beta).^2).*
(EpsR*k0^2-(beta).^2));

%Parametros de la radiating open end
%q=a/lambda0;
q=(k0^2-(beta)^2)^0.5*(a/(2*pi));

gamma=(sqrt(q^2-0.25));
gamma=real(gamma)-1i*abs(imag(gamma)); %Impongo el signo negativo

l=linspace(3,22,20);

Sm=zeros(1,20);
A=zeros(1,100);
A(1)=1;
for indice=1:20
Sm(indice)=sum(1./((l.*(l-1)).^(indice+0.5)));
A(2*indice+1)=(factorial(2*indice))./
(4^indice*factorial(indice)^2*(2*indice+1));
end

faux=zeros(1,20);
for indice=1:20
faux(indice)=A(2*indice+1)*Sm(indice)*gamma^(2*indice);
end

theta=2*(2-0.577+log(2/q)-(asin(gamma/q)/(2*gamma))-
(asin(gamma/sqrt(2))/gamma)+0.265-sum(faux));

R11_TEz_abs=sqrt((q-gamma)/(q+gamma))*exp(-pi*gamma);
```

```
R11_TMz_abs=sqrt((q+gamma)/(q-gamma))*exp(-pi*gamma);

Ti_TMz=-R11_TEz_abs*exp(-1i*theta); %cambio de signo
Tv_TEz=-R11_TMz_abs*exp(-1i*theta);

Zl_TEz=(sqrt(k0^2-kx^2-(beta)^2)/(w*Eps0))*((1+Tv_TEz)/
(1-Tv_TEz));
Yl_TMz=(sqrt(k0^2-kx^2-(beta)^2)/(w*Mu0))*((1+Ti_TMz)/
(1-Ti_TMz));

%Para una d muy grande las impedancias de radiacion seran las de
 las placas
%paralelas
Ya_vec_TMz=Y0_TMz*((1i*Y0_TMz+Yl_TMz*cot(ky_air*d))/(Y0_TMz*
cot(ky_air*d)+1i*Yl_TMz));
Za_vec_TEz=Z0_TEz*((1i*Z0_TEz+Zl_TEz*cot(ky_air*d))/(Z0_TEz*
cot(ky_air*d)+1i*Zl_TEz));

%Impedancias de la red PI y TEE
Y1_TMz=1i*Ye_TMz.*tan(ky*b/2);
Z1_TMz=1./Y1_TMz;

Y2_TMz=-1i*Ye_TMz.*csc(ky*b);
Z2_TMz=1./Y2_TMz;

Z1_TEz=1i*Ze_TEz.*tan(ky*b/2);
Y1_TEz=1./Z1_TEz;

Z2_TEz=-1i*Ze_TEz.*csc(ky*b);
Y2_TEz=1./Z2_TEz;

%Ecuaciones finales
out1=(Za_vec_TEz+Z1_TEz).*(Ya_vec_TMz+Y1_TMz+2*Y2_TMz)+N.^2;

out2=(Ya_vec_TMz+Y1_TMz).*(Za_vec_TEz+Z1_TEz+2*Z2_TEz)+N.^2;

out3=(Za_vec_TEz+1i*Ze_TEz.*tan(ky*b/2)).*(Ya_vec_TMz-1i*Ye_TMz.*
cot(ky*b/2))+N.^2;
out4=(Ya_vec_TMz+1i*Ye_TMz.*tan(ky*b/2)).*(Za_vec_TEz-1i*Ze_TEz.*
cot(ky*b/2))+N.^2;

DispRel=[Ya_vec_TMz+Y1_TMz+Y2_TMz Y2_TMz -N 0;
Y2_TMz Y0_TMz+Y1_TMz+Y2_TMz 0 N;
N 0 Za_vec_TEz+Z1_TEz+Z2_TEz Z2_TEz;
0 -N Z2_TEz Z0_TEz+Z1_TEz+Z2_TEz];
out=det(DispRel);

end
```

Appendix B

Matlab Codes:
nrd_leaky_function_main.m

```
clear all; close all;
global d;
global k0;
global a;
global b;
global EpsR;
global lambda0;
global f;

a=2.7e-3; b=2.4e-3;
EpsR=2.56;
f=48e9;


dist=linspace(6e-3,1e-3,200);

beta_vec=zeros(200,1);
betaref=573;
for i=1:length(dist)
    d=dist(i);

    betaref=cxroot(@nrd_leaky_function,betaref);
    beta_vec(i)=betaref;

end

figure(1);
```

```
plot(dist,real(beta_vec));
axis([0 6e-3 500 600]);
grid on;xlabel('d');ylabel('beta');

figure(2);
plot(dist,-imag(beta_vec));
grid on;xlabel('d');ylabel('alpha');

figure(3);
plot(dist,imag(beta_vec)/k0);
grid on;xlabel('d');ylabel('alpha/k0');

figure(4);
semilogy(dist,(abs(imag(beta_vec))));
grid on;xlabel('d');ylabel('alpha (dB/m)');

figure(5);
plot(dist,real(beta_vec)/k0);
axis([0 6e-3 0.4 0.7]);
grid on;xlabel('d');ylabel('beta/k0');
```